# INVESTIGATION OF TRIBOLOGICAL PROPERTIES OF GRAPHENE NANOPLATELETS REINFORCED METAL MATRIX NANOCOMPOSITES

**A Thesis Submitted to the**
**Graduate School of Engineering and Sciences of**
**İzmir Institute of Technology**
**in Partial Fulfillment of the Requirements for the Degree of**

**MASTER OF SCIENCE**

**in Mechanical Engineering**

**by**
**Seçkin MARTİN**

**June 2019**
**İZMİR**

We approve the thesis of **Seçkin MARTİN**

**Examining Committee Members:**

**Assoc. Prof. Dr. Sinan KANDEMİR**
Department of Mechanical Engineering, İzmir Institute of Technology

**Assist. Prof. Dr. M. Fatih TOKSOY**
Department of Mechanical Engineering, İzmir Institute of Technology

**Assist. Prof. Dr. Savaş ÖZTÜRK**
Department of Metallurgical and Materials Engineering, Manisa Celal Bayar University

**21 June 2019**

**Assoc. Prof. Dr. Sinan KANDEMİR**
Supervisor
Department of Mechanical Engineering
İzmir Institute of Technology

**Prof. Dr. Sedat AKKURT**
Head of the Department of
Mechanical Engineering

**Prof. Dr. Aysun SOFUOĞLU**
Dean of the Graduate School of
Engineering and Sciences

# ACKNOWLEDGMENTS

I would first like to thank my thesis advisor Assoc. Prof. Sinan Kandemir for the useful comments and his guidance through the learning and writing process of my master thesis. I would also like to thank Dr. Maksim Antonov who is the head of Research Laboratory of Tribology and Materials Testing at Tallinn University of Technology, for giving me the opportunity to work in their laboratory and sharing his knowledge.

I am especially grateful to my laboratory colleague, Neslihan Yağmur BÖBER for her support and assistance to my work.

Finally, I must express my very profound gratitude to my family and for providing me with unfailing support and continuous encouragement through the process of researching and writing this thesis. This accomplishment would not have been possible without them.

# ABSTRACT


## INVESTIGATION OF TRIBOLOGICAL PROPERTIES OF GRAPHENE NANOPLATELETS REINFORCED METAL MATRIX NANOCOMPOSITES

In this research, graphene nanoplatelets (GNPs) with a thickness of 50-100 nm have been utilized to improve the mechanical and tribological properties of A360 alloy due to their extraordinary mechanical properties and solid lubricant nature. During the fabrication process, GNPs were introduced into the liquid Aluminum (Al), then mechanical stirrer and ultrasonic treatment were used to obtain homogeneous dispersion of GNPs throughout the matrix. The examination of microstructures showed that A360/0.25 wt.% GNP nanocomposites have a relatively uniform distribution of GNPs. During the tribological properties investigation, ball-on disk tests were carried out at various temperature including room temperature (RT), 150°C, and 300°C. According to the hardness and ball-on-disk test results, the nanocomposite specimens exhibited improved hardness and wear resistance. The main mechanism of improvement in the hardness performance is mainly attributed the grain refinement by GNPs since they acted as the nucleation agents during the solidification process. The improvement in the wear behavior of nanocomposites could be referred to the temporarily formed solid lubricant film of harder GNPs during the wear, and hence coefficient of friction (COF) and volume loss results considerably reduced. Abrasive-adhesive, oxidation, and melting wear mechanism were found to be main mechanisms at RT, 150°C, and 300°C respectively. Overall, the results show that the nanocomposites fabricated by casting method combined with mechanical stirring and ultrasonication have promising wear performance, especially at elevated temperatures. This may suggest that these developed materials could be good candidates to be used in the engineering applications requiring high temperature wear performance.

# ÖZET

## GRAFEN NANOLEVHA TAKVİYELİ METAL MATRİSLİ NANOKOMPOZİTLERİN TRİBOLOJİK ÖZELLİKLERİNİN İNCELENMESİ

Bu çalışmada takviye malzemesi olarak, birkaç grafen tabakasından oluşan, 50-100 nm kalınlığa ve 5 μm ortalama çapa ve olağanüstü mekanik özelliklere ve katı yağlayıcı özelliğe sahip grafen nanolevhalar (GNL) kullanılarak A360 alaşımının mikroyapı ve değişik ortam sıcaklığındaki aşınma davranışlarının incelenmesi hedeflenmiştir. Döküm yöntemiyle üretilen bu nanokompozitlerin önündeki başlıca engel GNL'lerin geniş yüzey alanı ve yüksek yüzey enerjilerinden dolayı topaklanmaya eğilimli olmasıdır. Topaklanmayı engellemek adına master alaşım olarak sıvı fazdaki alüminyuma daldırılan GNL'ler daha sonra mekanik karıştırma ve ultrasonik proses ile matris içerisine homojen bir şekilde dağıtılma işlemi gerçekleştirilmiştir. Üretilen nanokompozitlerin iç yapı analizleri göstermektedir ki kütlece 0.25 oranında iç yapıya katılan GNL'lerin göreceli olarak homojen bir şekilde dağıtımı gerçekleştirilmiştir. Yapılan sertlik ve aşınma deneylerinde de, referans numunelere kıyasla GNL içeren nanokompozitler daha iyi performans sergilemiştir. Sertlik performansının iyileştirilmesinde ki temel mekanizma tane oluşumu esnasında GNL'lerin çekirdek oluşumu görevi görerek tane boyutlarını küçültmesine dayandırılmaktadır. Nanokompozitlerin aşınma davranışlarında ki iyileşme ise, GNL'lerin geçici olarak aşınma yüzeyinde katı yağlayıcı bir film tabakaları oluşturarak metal-metal temasını engellemesi ve bu sebeple sürtünme katsayısını düşürüp hacim kaybını azaltmasına dayandırılmaktadır. Ayrıca ortam sıcaklığına bağlı olarak aşınma mekanizmalarını belirlemek adına aşınan yüzeyler taramalı elektron mikroskobuyla incelenip raporlanmıştır. Oda sıcaklığında abrazif ve adhesif aşınma, 150°C'de oksidasyon aşınması ve 300°C de ise ergime mekanizması baskın aşınma mekanizmaları olarak tespit edilmiştir. Yapılan testler sonucunda, mekanik karıştırma ve ultrasonik proses yardımıyla üretilen nanokompozitlerin özellikle yüksek sıcaklık da aşınma davranışı gerektiren mühendislik uygulamalarında umut vaat eden bir aday olabileceği tespit edilmiştir.

# TABLE OF CONTENTS

# LIST OF FIGURES

**Figure** **Page**

**Figure** **Page**

# LIST OF TABLES

**Table** **Page**

# Chapter 1

# INTRODUCTION

Due to the friction and wear, reliability and lifetime of the engineering components could be affected negatively and hence they lead to a major impact on the economy. Considering the ground transportation, 208,000 million liters of fuel (diesel and gasoline) were only consumed in 2009 to overcome friction [1]. As seen in Figure 1.1, in passenger cars, one-third of fuel is used to overcome the friction of the components including engine, brakes, tyres and transmission equipments.

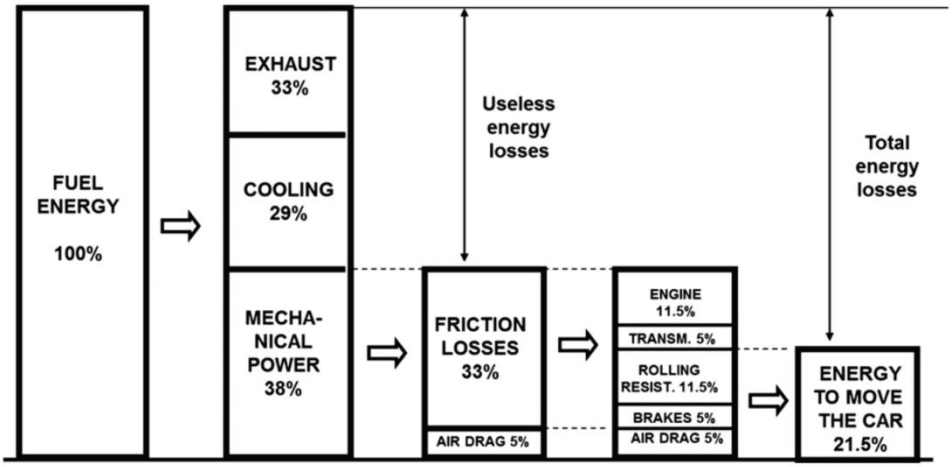


Figure 1.1. Schematic representation of energy dissipation in passenger car (Source: Holmberg et al., 2012)

In the case of a reduction in friction, both fuel consumption and $CO_2$ emission will be reduced. In order to tailor the friction of systems, several methods such as; low shear lubricants, advanced coating techniques or solid lubricants have been being developed for industrial applications.

On the other hand, in the past several decades, the use of lightweight alloys and their composites such as Al and magnesium (Mg), has been considered a promising option to contribute energy efficiency instead of traditional denser materials. Particularly, owing to Al and its alloys' high specific strength, high specific modulus, and low density, they are broadly employed in the automotive and aerospace industries

to reduce weight, hence energy consumption and $CO_2$ emission. Despite improved mechanical properties of Al alloys, the majority of these alloys suffer from their low hardness and wear resistance at elevated temperatures. The use of liquid lubricants is one of the most traditional solution methods to overcome friction and wear related issues in contacting bodies. However, reducing in COF and volume loss may not usually be obtained with the use of lubrication under challenging conditions, such as high temperature and high pressure. Therefore, many efforts have been spent to improve the wear resistance of Al alloys in order to meet the requirements in specific engineering application [2–4]. One of the preferred methods to enhance the wear performance of Al alloys is to reinforce them with a proper reinforcement material and fabrication technique i.e. composite technology. Numerous studies [5,6] have shown that the addition of micron-sized discontinuous reinforcement materials into Al matrices significantly enhanced the wear resistance of monolithic alloys. However, unlike the strength and wear resistance , the ductility tends to decrease in such composites. This limitation hampers the use of these wear resistant composites in broad engineering application areas. On the other hand, several studies [7–10] revealed that the addition of nano-sized ceramic and/or carbon-based reinforcement materials increased strength and wear resistance of the metal matrix without comprimising in the ductility.

In this research, graphene nanoplatelets (GNPs) which are the composed of few layer of graphene were used as the reinforcement material. As a carbon-based reinforcement material, graphene has become one of the promising and attractive reinforcement materials following the synthesis of graphene in 2004 due to its outstanding mechanical properties [11,12]. In addition, due to the weak van der Waals bonds, layered structure of GNPs could shear easily, and hence it can be expected that the incorporation of GNPs into metals has a solid lubrication effect on contact surfaces and could improve wear resistance.

The main aims of this thesis are to fabricate GNP reinforced Al matrix nanocomposites by casting which is suitable method for mass production, and examine the dry sliding wear behavior of the fabricated nanocomposites by means of ball-on-disk tests at various temperatures.

# Chapter 2

# LITERATURE REVIEW

## 2.1. Metal Matrix Composites (MMCs)

Composites are formed by combining at least two different physically and chemically phases by a suitable method and the properties of this structure are different from each those of constituents. Composites are composed of matrix and reinforcement phases. Generally, matrix are the continuous phases which play an important role in providing ductility and transferring the load to the reinforcement material. On the other hand, the reinforcement materials are generally discontinuous phases which are stiffer than the matrix, and thus contribute to the improvement of the mechanical properties of the composite.

Composites can be classified based on both matrix and reinforcement type. According to the matrix material, they can be divided into three groups and these are polymer, ceramic and metal matrix composites (MMCs). Since the subject of this thesis is MMCs, the focus will be on MMCs. In MMCs, the matrix is selected from metals or their alloys such as Aluminum (Al), Iron (Fe), Magnesium (Mg) or Copper (Cu).

The reasons for choosing metal matrix composites against monolithic alloys can be listed as follows [13].

- Weight reduction owing to the high strength to density ratio (spesific strength)
- Higher wear and fatigue resistance
- Dimensional stability
- Elevated temperature stability, i.e., creep resistance

Among the metal matrix materials, Al is the mostly used matrix material as depicted in Figure 2.1[14]. Owing to their high specific strength, high specific modulus ,and low density, Al and its alloys are widely used in the automotive and aerospace industries to reduce weight, hence energy consumption and $CO_2$ emission.

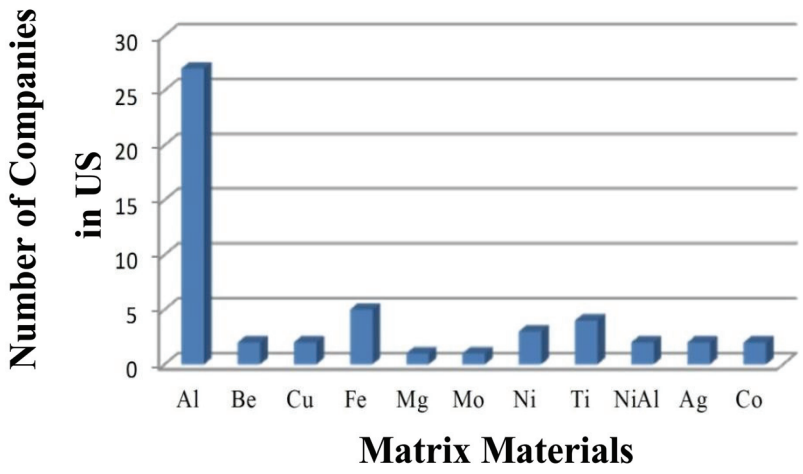


Figure 2.1. Number of companies that are using metals as a matrix material in their composite products (Source: Evans et al., 2003)

Depending on the selected matrix and reinforcement material, the properties listed previously can be improved. As an example, by adding a reasonable content of SiC into Al matrix, the strength and wear resistance of matrix could be enhanced. In addition, As seen in Figure 2.2, MMCs can be also grouped according to the form of the reinforcements. There are usually four types of metal matrix composites as listed below.

- Particle reinforced MMCs
- Short fiber or whisker reinforced MMCs
- Continuous fiber or sheet reinforced MMCs
- Monofilament reinforced MMCs[13,14]

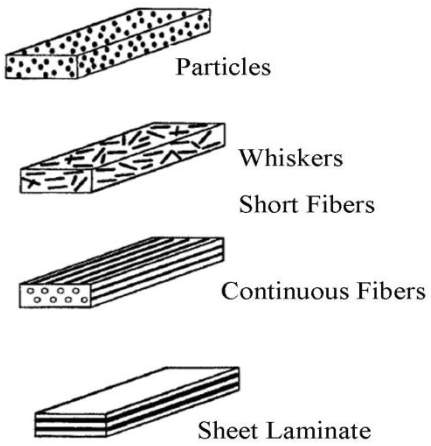


Figure 2.2. Different type of metal matrix composites (Source: Chawla et al., 2004)

### 2.1.1. Particulate Reinforced Metal Matrix Composites (PMMCs)

In PMMCs, mechanical properties of the metal matrix can be increased by adding micron-sized or nano-sized discontinuous reinforcement material. Considering the other types of metal matrix composite like continuous fiber or monofilament, the advantages of PMMCs can be summarized as listed below[14].

- Affordability of reinforcements
- Relatively cost-reduced production process
- Isotropy

When selecting the reinforcement material, parameters such as application area (temperature, corrosion, stress etc.), production method, and cost are taken into account in order to meet the desired properties. In general, it is expected that the reinforcement material embedded into the matrix material improves the wear behavior, high-temperature properties, and mechanical properties. Potential mechanical properties related to the type of reinforcement are given in the Table 2-1[15].

On the other hand, type, size, volume, wettability (in case of liquid state fabrication routes), physical properties and dispersion of reinforcement material are vital parameters affecting mechanical and physical properties of the MMCs. These topics will be discussed comprehensively in the following subheading.

Table 2-1 Potential mechanical properties of different type of MMCs (Source: Kainer et al., 2006)

| MMC Type | Properties of Strength | Young's Modulus | High Temperature Properties | Wear | Expansion Coefficient | Costs |
|---|---|---|---|---|---|---|
| Mineral wool: MMC | * | * | ** | ** | * | Medium |
| Discontinuous reinforced MMC | ** | ** | * | *** | ** | Low |
| Long fiber reinforced MMC: C fibers | ** | ** | ** | * | *** | High |
| Other fibers | *** | *** | *** | * | ** | High |

## 2.1.2. Reinforcement Type

When the particle-reinforced metal matrix composites are evaluated in terms of the reinforcement material, ceramics primarly stand out as the main reinforcement material due to high stiffness, low density, and relatively low-cost. In addition to the ductility of the matrix material, the strength of the composite can be increased by the incorporation of ceramic reinforcement material, and such composites are broadly used in the aviation and ground transportation industries.

Depending on the application area of PMMCs, the ceramic reinforcement materials could be oxides ($Al_2O_3$, MgO), borides ($B_4C$, $TiB_2$), and carbides (SiC, TiC) [16].

The industrial application areas of ceramic reinforced metal matrix composites produced by casting method were shown in Table 2-2 [17]. The wear behavior of the matrix materials can be improved by the ceramic reinforcement material. However, the relatively rigid/hard ceramic reinforcement material included in the tribo-film formed during the wear operation can lead to an increase in the wear rate of both the matrix material and the counter-material [18,19].

Table 2-2 Industrial examples of casted PMMCs

| Companies | Components and Composites |
|---|---|
| Duralcan, Martin Marietta, Lanxide | Pistons, Al/SiCp |
| GKN, Duralcan | Propeller shaft, Al/SiCp |
| Dupont, Chrysler | Connecting rods, $Al/Al_2O_3$ |
| Associated Engineering, Inc. | Cylinders, pistons, Al/graphite |
| Martin Marietta | Pistons, connecting rods, $Al/TiC_p$ |
| Honda | Engine blocks, $Al/Al_2O_3 - C_f$ |
| Lotus Elise, Volkswagen | Brake rotors, $Al/SiC_p$ |
| Cercast | Electronic packages, Al/graphite foam |

In addition to ceramic reinforcement materials, carbon-based reinforcement materials (graphite, graphene) are also a promising option to tailor mechanical properties of matrix material thanks to their high damping capacity, high thermal conductivity, and low coefficient of thermal expansion [2]. Further, due to their solid lubricant effect, carbon-based reinforcement materials are also widely used to reduce

COF and improve the wear behavior of matrix material. However, there are certain limitations in the use of graphite as a reinforcement material.

First of all, graphite needs a humid environment to show the solid lubricant feature. The reason for providing a low coefficient of friction in humid environments is the penetration of water molecules between the graphite sheets so that the graphite sheets are easily sheared and the friction coefficient is reduced by covering the worn surface [20]. As shown in the Figure 2.3, graphite exhibited reduced coefficient of friction results in a humid environment than the dry environment [20]. On the other hand, it has no major effect of reducing the friction coefficient and wear rate in dry or vacuum environment. Additionally, numerous resarches revelad that[21,22] the mechanical properties of the matrix material are adversely affected depending on the graphite content. The critical point to consider when selecting the reinforcement material is that mechanical properties are not compromised while improving wear behavior. Several studies[7–10,23] showed that the addition of nano-sized ceramic and/or carbon-based reinforcement materials increased strength and wear resistance of metal matrices.

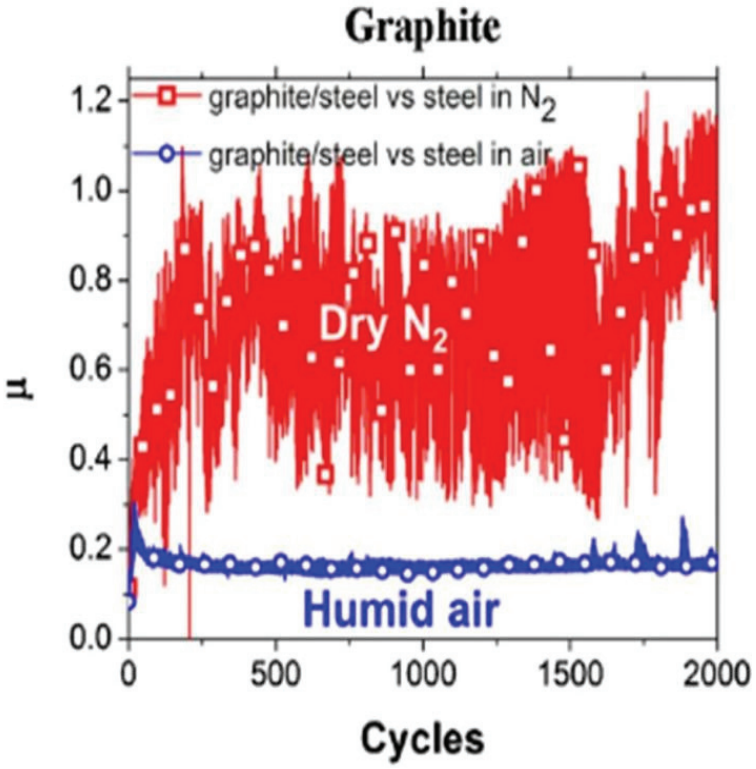


Figure 2.3. Effect of environmental factors on wear behavior of graphite (Source: Baradeswaran et al., 2015)

**Graphene**

Graphene is a monolayer carbon allotrope with a hexagonal lattice structure. Graphite, fullerene and carbon nanotube (CNT) can also be obtained as a result of variations such as rolling or overlapping of graphene [24] (See Figure 2.4).

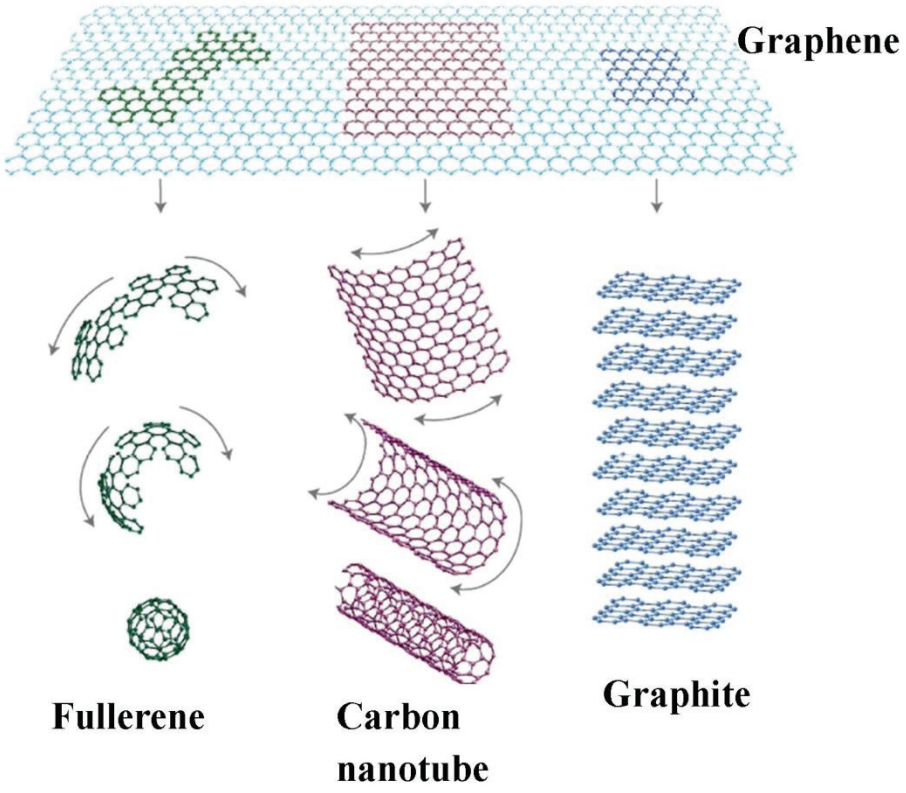


Figure 2.4. Schematic drawing of graphene and its allotrope
(Source: Randviir et al., 2014)

Graphene has become one of the promising and attractive reinforcement materials following the first synthesis of graphene in 2004 due to its outstanding mechanical properties as seen in Table 2-3[11,12].

Table 2-3. Mechanical properties of Graphene

| Property | Graphene |
|---|---|
| Elastic Modulus | 1 ~TPa |
| Fracture strength | 125 GPa |
| Thermal Conductivity | 4840-5300 W/mK |

Moroever, the reason for being a promising reinforcement material is that its improved mechanical properties as well as it is used to develop the wear behavior of materials due to the nature of the solid lubricant. [25]. Figure 2.5 confirms that the use of graphene as a solid lubricant is one of the hot topics in the literature over the last two decades.

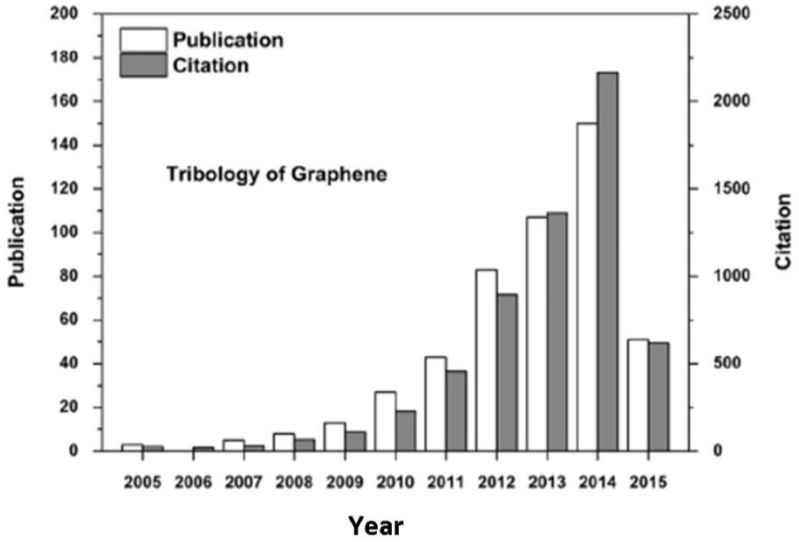


Figure 2.5. Publications related with graphene and tribology
(Source: Dong et al., 2015)

However, it is the fact that graphene can rarely remain stable as a single layer, therefore, it is widely employed as graphene nanoplatelets with a thickness of fewer than 100 nanometers [8,26]. In addition, due to the weak van der Waals bonds, layered structure of graphene nanoplatelets (GNPs) could be sheared easily, and hence it can be expected that the incorporation of GNPs into metals may result in solid lubrication effect on contact surfaces. Several studies have shown that[26,27] GNPs have been proved to be a good candidate to improve the wear behavior of aluminum matrix composites due to its solid lubricant nature. However, the wettability and the content of the reinforcement material to be incorporated are vital parameters affecting the mechanical and tribological properties.

***Wettability***

The interface between the matrix material and the reinforcement material is of vital importance in determining the mechanical behavior of metal matrix composites fabricated by solidification based routes e.g, casting. While any defects such as porosity on the interface affect the load transfer between the matrix and reinforcement

negatively, a clean interface and strong bonding increases the strength of composites. For these reasons, wettability and interface conditions are the parameters that need to be improved. From this point, the interaction between aluminum and some carbon reinforcement materials will be examined.

In order to enlighten the wettability of a reinforcement material by molten metal, Young-Dupre developed a model ( see Figure 2.6.). According to that model, wetting angle can be calculated by Equation 2.1 [28]:

$$cos\theta = \frac{\gamma_{sv}-\gamma_{sl}}{\gamma_{lv}} \tag{2.1}$$

where $\gamma_{lv}$ is the surface energy of the liquid, $\gamma_{sl}$ the interface energy between the liquid and solid base, $\gamma_{sv}$ the surface energy of solid and $\theta$ is the contact angle. As can be ascribed from the Figure 2.6, when the contact angle exceeds $\pi / 2$, the wettability of the system is not sufficient and when the contact angle is below $\pi / 2$, the wettability of the system can be interpreted as adequate. In the liquid state process, The work-energy among liquid-solid phase per unit area in carrying out this operation is called the work of adhesion and according to Equation 2.1 :

$$W_a = \gamma_{lv} + \gamma_{sv} - \gamma_{sl} \tag{2.2}$$

$$Wa = \gamma_{lv}(1 + \cos\theta) \tag{2.3}$$

According to Equation 2.3, work of adhesion is the function of the contact angle and the surface energy of the liquid.

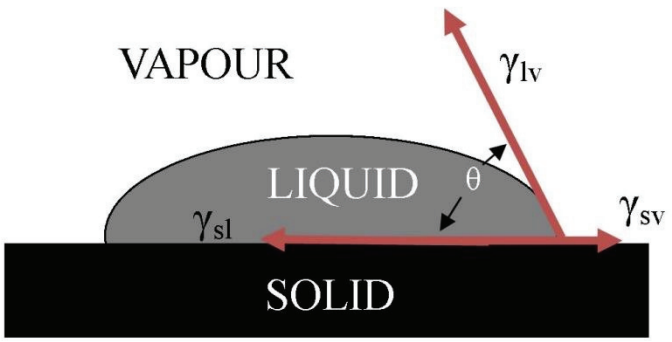


Figure 2.6. Schematic drawing of the wetting angle of a droplet on a solid base

Wetting carbon-based reinforcement materials, such as graphite, CNT, GNPs, with aluminum is a challenging task [15,29]. According to the literature [30], the range of contact angle between graphite (bulk graphene) substrate and liquid aluminum is between 140° and 160° (see Figure 2.7). This result shows that the aluminum in the liquid phase has low wettability due to the high surface tension.

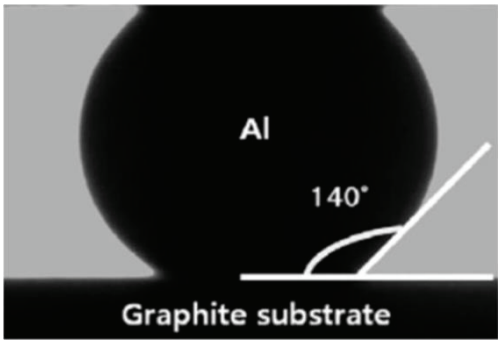


Figure 2.7. Contact angle between Graphite substrate and liquid Aluminum (Source: Nuriel et al., 2005)

There are various methods reported in the literature to increase the wetting of the aluminum matrix in the liquid phase. In order to enhance the wettability of aluminum matrix magnesium, titanium, and chromium are incorporated into the liquid phase [31]. Alternatively the wettability of reinforcement could be improved. For example, graphite (bulk graphene), it is coated with copper and hence the wettability angle is reduced [30]. Cu is utilized as a coating since it is chemically stable with carbon and could reduce the formation of undesirable $Al_4C_3$ compound in carbon/matrix interfaces [32].

### 2.1.3. Strengthening Mechanism of PMMCs

In this study, the strengthening mechanisms of nanomaterials will be scrutinized since nano-sized GNP is employed as reinforcement material. Regarding the strengthening mechanisms of nano-sized reinforced MMCs, four different strengthening mechanisms listed below play an active role in improving mechanical properties.

- Orowan strengthening
- Hall-Petch (Grain-boundary) strengthening
- Load transfer by reinforcement
- Coefficient of thermal expansion mismatch (CTE)

Basically, reinforcement materials embedded into a matrix hinder the movement of dislocations. According to Orowan strengthening mechanism[33], the dislocation encountered with the particle surrounds the particle and, in contrast to passing through the particle, makes bow first and returns to its original form as illustrated in Figure 2.8.

In the case where the reinforcement material is in micron size, Orowan

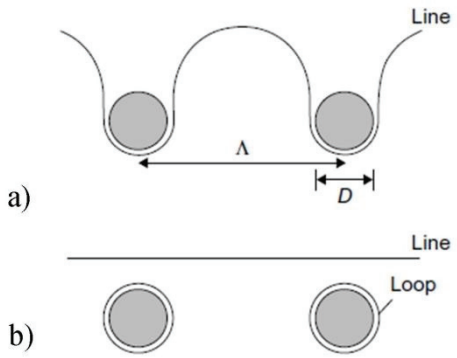


Figure 2.8. Schematic drawing of Orowan strengthening mechanism a)The line bows between the obstacles b) Orowan loops (Source Bacon, 2011)

strengthening mechanism has no significant effect on the improvement of mechanical properties [34]. In contrast, with the addition of reinforcement materials smaller than 100 nm, Orowan strengthening mechanism was found to be more beneficial to tailor the mechanical properties of MMCs [35].

Hall-Petch strengthening mechanism is essentially related to grain refinement. Reinforcement materials affect the grain size during grain formation since they can act as a pinpoint at grain boundaries or stop growth [36]. The effect of refinement of grain size to yield stress can be found in the following Hall-Petch equation [33].

$$\sigma_y = \sigma_0 + k_y d^{-n} \quad (2.4)$$

where exponent n is approximately 0.5, $k_y$ is a material constant and $\sigma_0$ initial yield strength. Therefore, the grain size of the material *d* is the only variable that affects the yield stress.

In general, it is known that during solidification in case of liquid state routes CTE mismatch between the metal matrix and the reinforcement phase can cause plastic strains and they increase the density of the dislocation hence the strength. The strengthening mechanism of CTE can be described by the following equation[2].

$$\Delta\sigma_y = \alpha G b \rho^{-1/2} \quad (2.5)$$

where α is a constant, G the shear modulus, b the Burgers vector of dislocations and ρ the density of dislocations.

## 2.1.4. Processing Methods of PMMCs

Depending on the form of the reinforcement material, the favorability of the production method to both the matrix and the reinforcement material, MMCs can be grouped into 3 main headings as shown in the Figure 2.9 [14].

Among these production methods, the commonly used methods for the production of PMMCs are liquid-state and solid-state processes.

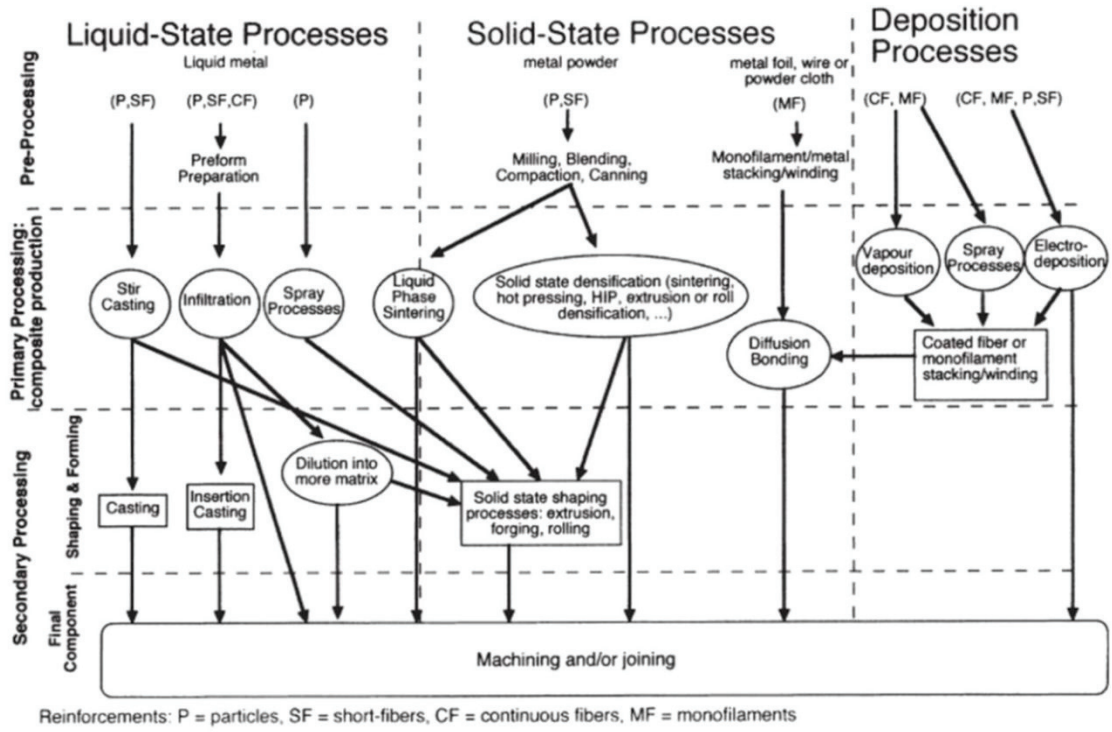


Figure 2.9. Processing type of MMCs (Source: Evans et al., 2003)

***Solid state process***

Among other methods stated in Figure 2.9, powder metallurgy (PM) is a widely used method in the solid-state processes. PM is briefly based on the blending of the powders of the matrix and the reinforcement material under suitable conditions, then increasing the density of these mixed powders by the pressing (cold-compacted or hot-

pressed), and finally forming the metal matrix composites by applying the forming operations such as rolling, extrusion or forging [13].

Since the powder metallurgy method does not reach high temperatures (melting point of matrix) like casting processes, it is unlikely to occur interface reactions between matrix and reinforcement material. However, PM method may not be suitable for mass production and, besides being expensive, densification problems are the major obstacles to the widespread use of PM in the industry.

***Liquid state process***

There are various ways of physically combining reinforcement and matrix materials in liquid state. Nowadays, Liquid-state processing methods are being investigated and widely used methods are [37].

- Stir Casting
- Infiltration processes
- Spraying
- In-situ process

One of the major advantages of the traditional casting process is that it reduces production cost in large volumes. However, the wettability of reinforcement by liquid metal is one of the main problems. Particularly in this study, the wetting of aluminum matrix used in the casting process is relatively low due to its high surface energy [29]. As mentioned earlier, some methods have been developed to overcome these shortcomings, such as adding alloying elements to the liquid metal and coating of reinforcement material. Furthermore, nano-sized reinforcement materials tend to agglomerate shortly after reinforcement is incorporated due to their high surface-to-volume ratio. During the fabrication of nano-sized reinforced MMCs, stir casting does not provide sufficient energy to attain homogenous dispersion of nano particles due to their agglomeration tendency. Therefore, the ultrasonic processing technique has been considered a promising method to provide a uniform distribution and to disperse possible clusters of nano-sized particles. The acoustic processing technique consists of acoustic cavitation and acoustic streaming. It is believed that in the process of acoustic cavitation, generated bubbles collapse or hit to the potential reinforcement clusters, and thus may induce seperation of nanoparticles. During the acoustic streaming, broken up nanoparticles and bubbles dispersed through the liquid metal, and hence lead to uniform distribution of nanoparticles. Further, circulated bubbles could play a significant role in

grain refinement by preventing dendrite formation during the solidification. Schematic presentation of the acoustic processing technique can be seen in Figure 2.10.

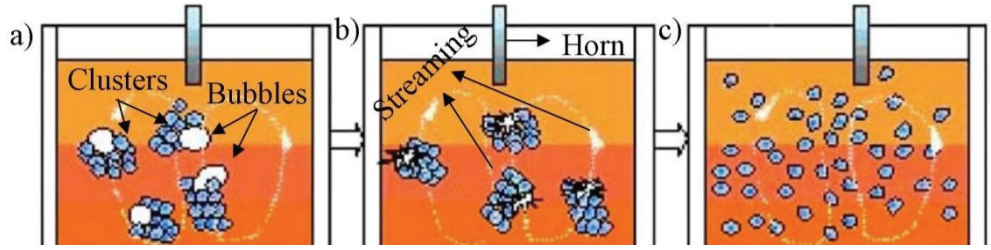


Figure 2.10. The acoustic processing a) growth of bubbles, b) collapsing of bubbles, and c) break-up and re-dispersion of nanoparticle clusters (Source: Lan et al., 2004)

## 2.2. Wear

Basically, the definition of wear is to damage to a solid surface. More specifically, wear is defined as the mass loss of material from the surface and/or transfer of material from one surface to another during the motion [38]. In order to determine wear behavior of materials, several methods are avaliable in literature. As illustrated in Figure 2.11[39], pin-on-disk, block-on-ring, reciprocating, twin disk, and ring-on-ring tests are most common method to investigate wear behavior of materials in a laboratory

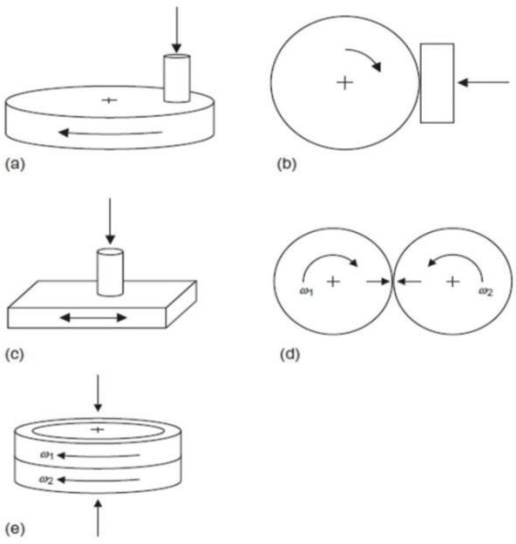


Figure 2.11. Configurations of wear tests (Source: Hutchings et al., 2017)

environment.

Prior to starting test, standards of these test configurations must be obtained. For example, requirements of pin-on-disk test can find from the ASTM G99-05 standards.

The wear behavior can be observed in parts that work together such as piston-cylinder systems, gas turbines, bearings, etc. As with the examples, in most engineering applications, wear and COF along with lubricant can be kept to a minimum or at least controlled, and such systems are called *lubricated sliding wear*. However, in the laboratories or in some engineering applications, wear behavior without lubricant is also examined, which is called *dry-sliding wear*. Based on the contact types, deformation states, and wear types, the wear chart is constructed as seen in Figure 2.12 [40].

Since the subject of this thesis is dry-sliding-wear behavior MMCs, this issue will be discussed in following sections. As illustrated in Figure 2-12, during the dry-sliding, mechanical and chemical mechanisms should be known to determine the wear behavior of the system. For instance, wear could be done by solely mechanical such as

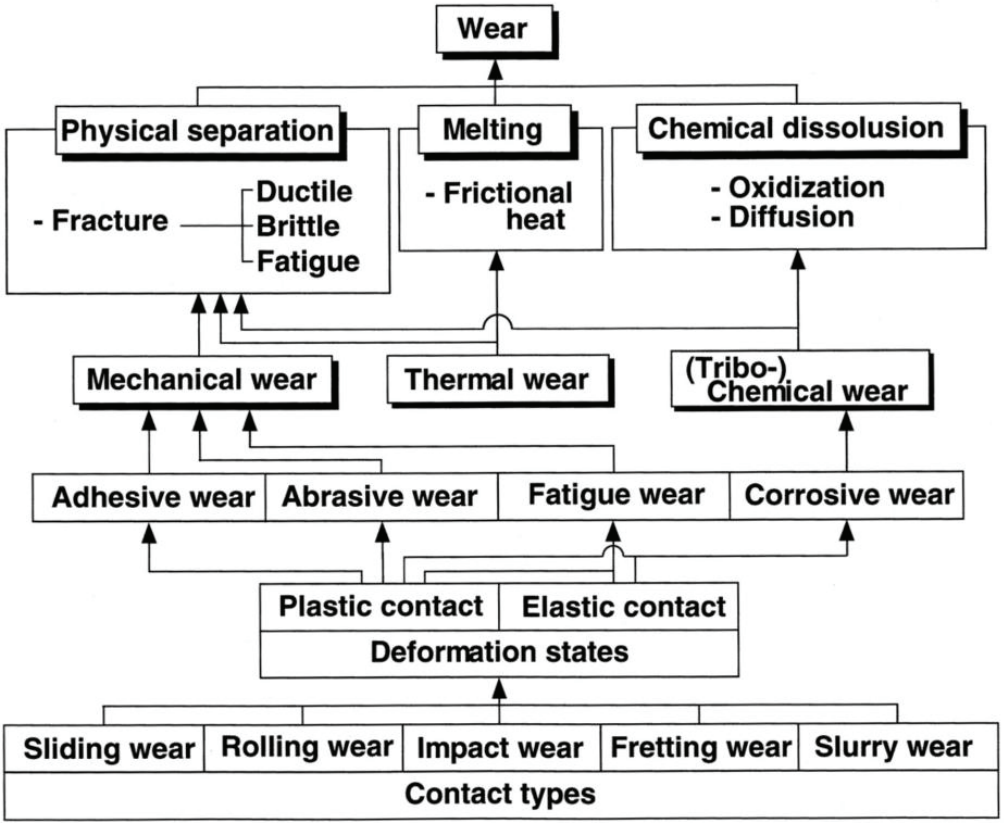


Figure 2.12. Wear Chart (Source: Kato et al., 2001)

involving plastic deformation or brittle fracture, or they may include significant chemical aspects, for example, oxidation of a metal due to the environmental factors. However, in real life, many applications consist of the combination of chemical and mechanical process.

Generally, most mating surfaces lose their precision, reliability, and durability due to wear. Therefore, modeling and estimating of the wear behavior of materials have become an important requirement for the development of new technologies.

Archard is the first person who formulates parameters that affect wear behavior. According to the Archard equation [41];

$$Q = \frac{KW}{H} \tag{2.6}$$

where Q is the volume taken away from the surface per unit sliding distance, W is the normal load and H is the indentation hardness of the wearing surface. K is the *wear coefficient* and it is unitless. It has an effective factor in determining the severity of the wear.

As shown in Figure 2.13, K alters under different working conditions [38]. The use of liquid lubricants is one of the most traditional solution method to decrease wear effect on systems, however, reducing in coefficient of friction and volume loss may not be obtained under challenging conditions, such as high temperature, high pressure. For this reason, solid lubricants that adapt to demanding conditions and improve wear

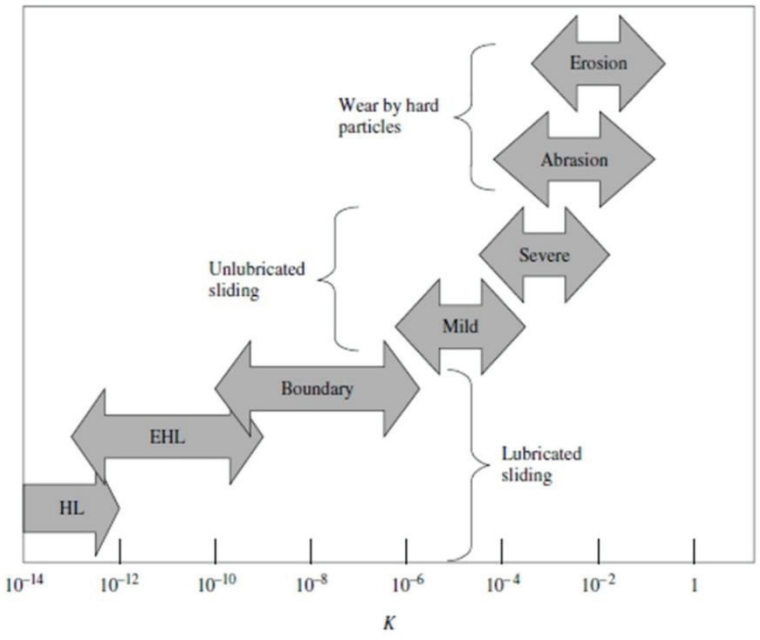


Figure 2.13. Wear HL=hydrodynamiclubrication; EHL = elastohydrodynamic lubrication (Source: Stachowiak et al., 2004)

behavior are becoming considerable day by day.

***Mild wear***

Mild wear generally defined as an oxidative phenomenon of growth and spalling of oxide at the asperity level. So, during the mild wear mating surface are separated by oxide layers. The severity of wear could be detected from such parameters including the rates of wear, surface morphology and wear debris. In mild wear, low wear rate, smooth surface morphology, and fine oxide particles are the dominant proofs to deduce wear type of system.

***Severe wear***

During the wear, high plastic deformation and destabilizing of protective oxide layers are the evidence to deduce the wear transition from mild to severe. As seen in Figure 2.13, K is generally in between $10^{-3}$ and $10^{-2}$ which is unacceptable in engineering applications. Observation of relatively high wear rate, deformed and rough surface morphology, and coarse metallic flakes could help to predict whether severe wear mechanism.

In particular, during the dry-sliding wear, the effect of solid lubricant may help to keep the wear regime under mild regime instead of severe regime, and hence damage on a mating surface may be decreased. Wear modes will of metals be scrutinized in following sections.

## 2.2.1. Wear Modes

During the dry-sliding wear of metals, various types of damage can be observed as follows;

- Microstructural changes under the wear surface due to mechanical deformations and thermal effects
- Wear layer, chemically different from both surfaces, formed between contact surfaces.
- Particulate material, technically wear debris, is broken away from the contact surface.

A worn metal surface is modeled in Figure 2.14[40]. In order to determine the circumstances listed above, OM, SEM (equipped with Energy-dispersive X-ray,

Backscattered electron, and Secondary electron detectors), and TEM are used. By means of these types of equipment, it is allowed us to attain chemical and structural

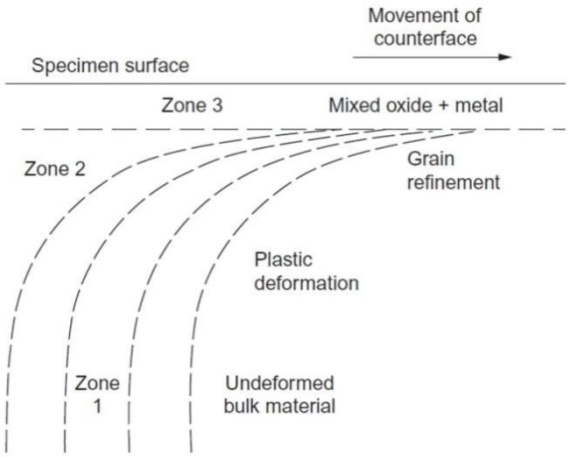


Figure 2.14.Schematic drawing of worn metal surface (Source: Kato et al., 2001)
information about the wear modes and wear debris from worn surfaces.

During wear, different wear mode or modes can dominate the process. In general, the wear modes acknowledged in literature are as follows:

- Adhesive wear
- Abrasive wear
- Fatigue wear
- Corrosive wear

Briefly, the schematic view of modes can be seen in the Figure 2.15, and information about the modes will be described in the following topics.

***Adhesive wear***

At the beginning of wear, adhesion occurs between asperities and due to the

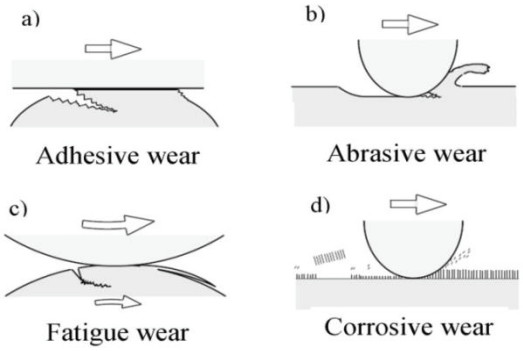


Figure 2.15. Drawing of wear modes, a) adhesive, b) abrasive, c) fatigue, and d) corrosive wear

movement, the contacting surfaces connected to each other are forced to separate. Due to the plastic deformation, crack is started from under the worn surface and is spread. When the crack reaches the worn surface, it is transferred to the other surface and wear is completed. So, transferring material from a softer surface to a harder surface or loss from either surface is called adhesive wear. Mechanism of adhesive wear can be seen in Figure 2.15 a). When the presence of delamination patches on the worn surfaces is detected by means of SEM, it implies that the dominant wear mode is adhesive wear.

***Abrasive wear***

Due to the hard particles that exist before wear or occur during the wear (oxides), counterface suffers damage during the sliding. Depending on materials type abrasive wear could result in either plastic deformation or fracture. For ductile materials such as Al, hard particles induce ploughing marks on the surface by plastic deformation. On the other hand, fracture occurs during the sliding against brittle material. Abrasive wear usually occurs in two types including two-body and three-body abrasion as shown in Figure 2.16 [39].

The main difference between two and three-body abrasion is, in the case of two-body abrasion, hard particles are embedded or attached to counterface. However, in the

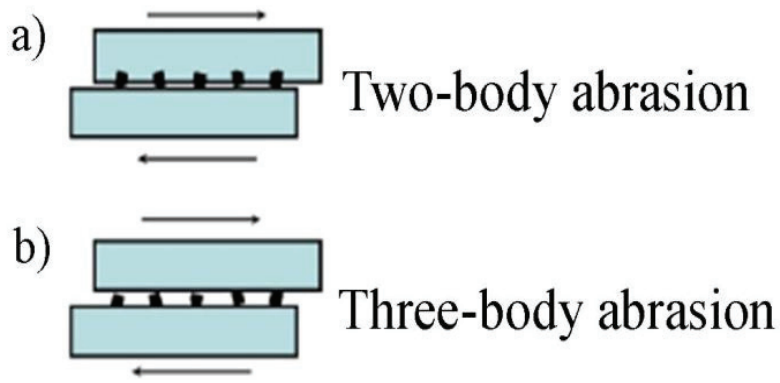


Figure 2.16. Types of abrasive wear, a) Two-body abrasion, and b) three-body abrasion

case of three-body abrasion, particles can slide and roll among mating surfaces.

***Fatigue wear***

During the repeated sliding and loading cycles could provoke crack initiation under the surface and hence wear occurs due to the fracture. This type of wear is called fatigue wear. Fatigue wear can take place either plastic contact or elastic contact as seen in Figure 2.12. can be observed in two different types which are high-cycle and low-

cycle fatigue. If the critical number of cycle is high, it is called high-cycle fatigue mode. When it is low, low-cycle fatigue mode is expected to happen on worn surface.

***Corrosive wear***

Metals usually have a high affinity for oxygen. Therefore, their surface is covered with a thin oxide film in an atmospheric environment. During the wear, deattached oxide particles from the surfaces of mating materials make the rest of surfaces are vulnerable to oxidation due to continuous wear. This type of wear is called corrosive wear.

## 2.2.2. Factors affecting Wear Behavior

Microstructural changes under the wear surface due to mechanical deformations and thermal effects could affect the severity of the wear. Parameters including load, sliding velocity, time-distance, and temperature should be controlled to avoid gross wear damages between mating couples [38]. Based on the normalized pressure, normalized velocity, and sliding velocity the severity of the wear of steel could be predicted, as shown in Figure 2.17. Further, this graph could be utilized for the depiction of other metals due to the similarities in dry-sliding wear behavior of metals in air [39].

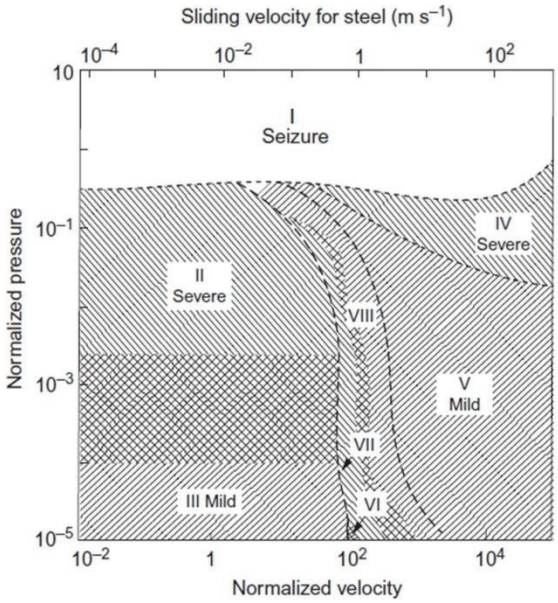


Figure 2.17. Wear mode map for the dry-sliding of steel in the pin-on-disc configuration (Source: Hutchings et al., 2017)

On the other hand, temperature is one of the critical parameters that affect the wear behavior of engineering components. At room temperature tests, micro-cracks, which grow leading to material loss in the form of flakes and abrasive wear could play a significant role, while plastic deformation and unstabilized oxide layer could be seen as a result of elevated temperature tests.

In this research, unreinforced alloy and AMNCs were tested by means of ball-on-disk tests to insvestigate the elevated temperature effect on wear behavior of such composites.

# Chapter 3

# EXPERIMENTAL DETAILS

## 3.1. Materials

In this study, A360 alloy was selected as the matrix material. The chemical composition of A360 was given in Table 3.1.

The addition of Silicon (Si) excessively imparts liquidity and hot tear resistance to aluminum alloys. Therefore, the presence of relatively high Si content makes A360 alloy preferable as the matrix material for casting [42]. Furthermore, when molten aluminum is overheated, it tends to form $Al_4C_3$ brittle phase by reacting with GNPs, a carbon-based reinforcement material (Equation 2.5), hence Si has a vital role in suppressing the chemical reaction between carbon and aluminum[43].

$$4Al + 3C \rightarrow Al_4C_3 \quad (2.5)$$

Additionally, $Al_4C_3$ also makes the aluminum matrix vulnerable to corrosive environments [43].

Graphene nanoplatelets having a thickness of 50 - 100 nm, a diameter of 5 μm and a purity of 96-99% were obtained as a reinforcement material from Grafen Chemical Industries. The SEM micopraph of GNPs can be seen in Figure 3.1. In addition, in order to prevent the agglomeration of GNPs during the feeding process, aluminum and magnesium powders of 99% purity and an average size of $\leqslant$ 75 μm were utilized to form master alloy produced by planetary ball-milling with the GNPs.

Table 3.1. Chemical composition of A360 alloy (wt.%).

| Al | Si | Fe | Cu | Mn | Mg | Zn | Ti |
|---|---|---|---|---|---|---|---|
| Bal. | 10.0 | 0.50 | 0.1 | 0.5 | 0.35 | 0.1 | 0.15 |

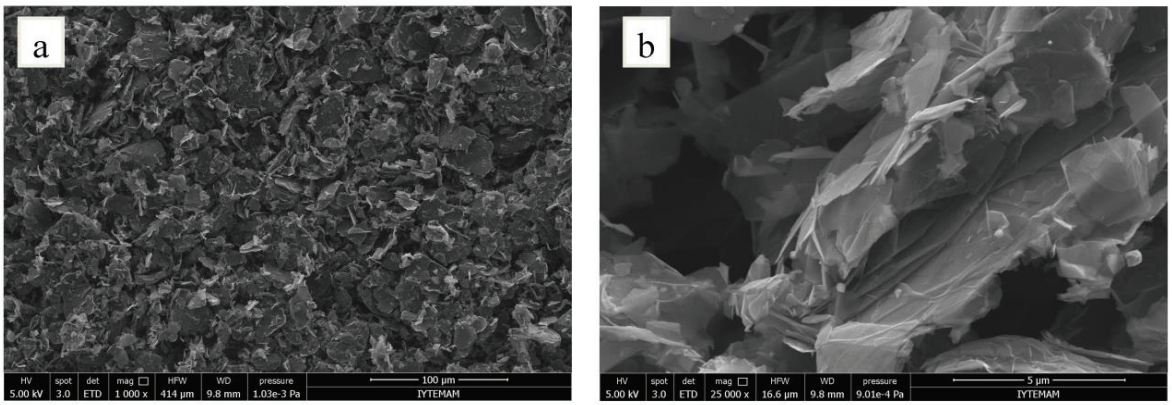


Figure 3.1. a) Low and b) high magnification SEM images of the GNPs used in this study

## 3.2. Fabrication of Aluminum Matrix Nanocomposites

Prior to starting the casting process, in order to hinder the agglomeration of the reinforcement material, GNPs were blended with the aluminum and magnesium powders together by means of the ball-milling process. As shown in Figure 3.2, Retsch PM100 ball miller was utilized. During this process, aluminum and magnesium powders of 99% purity were used to enable GNPs to be effectively incorporated into the liquid metal.

The main purpose of adding magnesium powder is to reduce the surface tension of the molten aluminum having a relatively high surface tension and to increase the wettability of GNPs by the molten alloy [31]. Ball milling operation was carried out for an hour at 350 rpm. During the ball milling operation, stainless steel balls with a diameter of 10 mm were utilized and ball to powder ratio was set to 9:1.


Figure 3.2. Planetary ball milling machine


Figure 3.3. Hydraulic press

In the literature [7-10], it has been observed that the addition of a few amounts of nano-sized reinforcement materials to the matrix results in improved mechanical and abrasion behavior. For this reason, when ratios of GNPs (wt.%) were determined, the GNP contents in composites were set to be about 0.25 and 0.5 wt % for a different set of samples by taking into account the agglomeration problem. The powders and GNPs mixed with ball milling process were combined with the cold compacted method and converted into 30 mm diameter tablets under 250 MPa (see Figure 3.3). The purpose of using tablets is to prevent the floating of the GNPs on the molten metal surface due to the density difference. The experimental setup can be seen in Figure 3-4. A360 alloy was cut into small ingots and 200 g of the alloy was then placed into a graphite crucible. Once the alloy was completely melted by heating at 650 °C and the tablet feeding process was launched. After the feeding procedure, mechanical stirring was applied for 15 min. at 400 rpm in order to lead to the erosion of tablets and hence distribute the GNPs through the matrix as seen in Figure 3.4a. Then, the molten alloy was reheated up to 675°C to apply 15 min. ultrasonic treatment with an ultrasonic device (Q700-Qsonica, LLC) to obtain homogeneous distribution and dispersion of GNPs (Figure 3.4b). After the distribution process was accomplished, the ultrasonic probe was removed and the liquid composite was casted into a pre-heated permanent steel mold. The GNP contents were set to be about 0.25 and 0.5 wt. % in composites. The reference alloy without the addition of GNPs was also fabricated with the same

fabrication method followed for the aluminum matrix nanocomposites (AMNCs) in order to observe the potential individual effects of GNP on the alloy.

After the fabrication process, AMNCs were turned into ball-on disk samples by using turning steps. Before starting the ball-on-disk tests, samples were ground and polished to 1 μm surface finish.

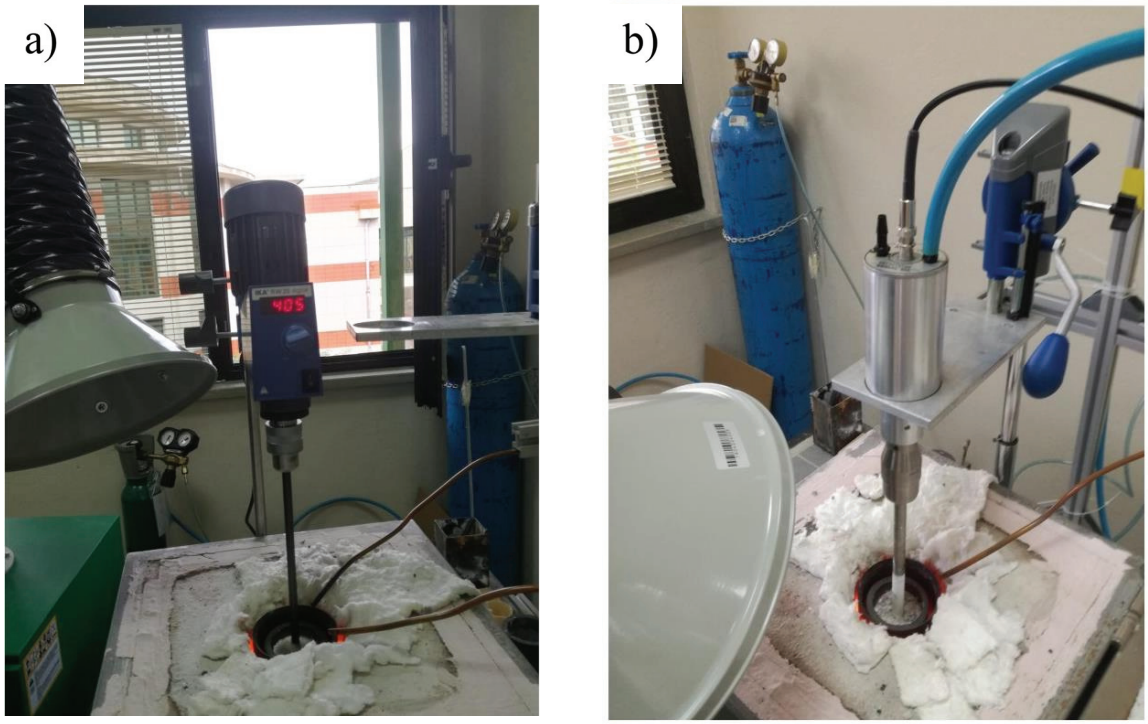


Figure 3.4. a) Mechanical stirrer b) Ultrasonic treatment from the experiment

## 3.3. Hardness Tests

Vickers hardness (HV) tests were performed to investigate the effect of GNPs on hardness via Shimadzu Microhardness Tester. Five tests were performed for each sample and average results were reported. The results will be discussed in detail in Chapter 4.

## 3.4. Ball-on-disk Tests

In order to investigate the dry sliding wear-behavior of the aluminum matrix nanocomposites (AMNCs), ball-on-disk (CETR-Bruker) tests were conducted against a

counter face AISI 52100 (62 HRC) steel ball with a diameter of 10 mm. Test setup was shown in Figure 3.5.

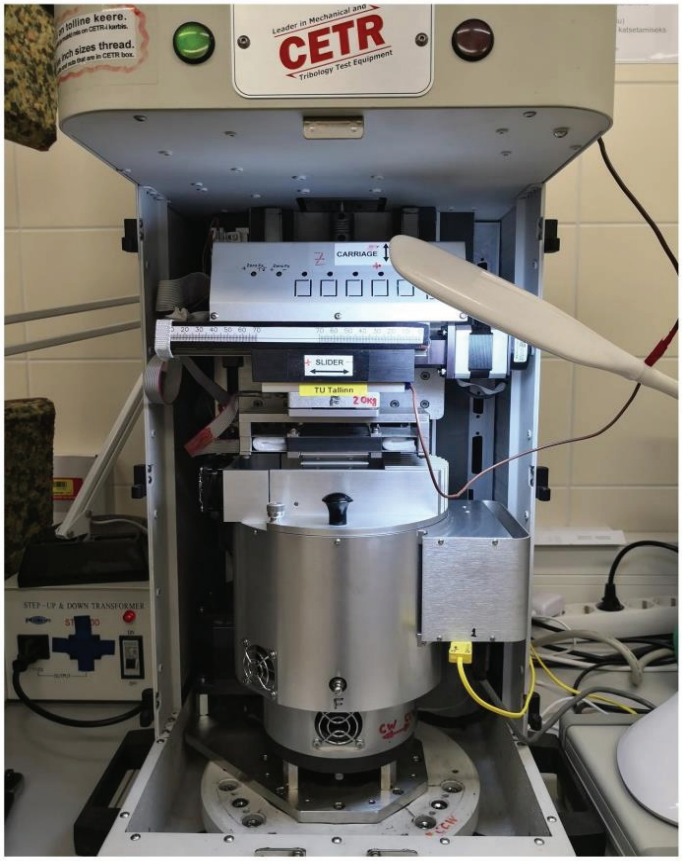


Figure 3.5. Ball-on-disk test setup

Ball-on-disk test parameters also were given in Table 3-2.

Table 3.2. Parameters of ball-on-disk tests

| Steps | Load (N) | Duration (min.) | Speed (rpm) | Temperature (°C) |
|---|---|---|---|---|
| Track generation | 20 | 1 | 1 | Room Temperature (RT), 150°C, 300°C |
| Run-in | 2 | 1 | 273 | RT, 150°C, 300°C |
| Long test with stops (7 stops) | 2 | 83 | 273 | RT, 150°C, 300°C |

It was aimed to examine the dry sliding wear-behavior of AMNCs by selecting 3 different test temperatures that were RT, 150°C, and 300°C. Several studies have shown that aluminum alloys cannot remain stable beyond 250°C [44]. Therefore, the test temperatures were selected to be above and below the critical temperature. The load was selected as 2N and kept constant during the tests due to limited mechanical properties. The Hertz contact stress was estimated to be 380 MPa which was nearly to the equal

compressive stress of reference alloy. For that reason, ball-on-disk test was designed with three different steps including track generation, run-in and long test with stops. In the track generation stage, the sample surface was lubricated with a suitable oil (Exxonmobil spectraSyn 8) to prevent excessive plastic deformation. After this stage, the lubricant immediately washed out with acetone and ethanol. In the second step, run-in, the sample was worn for only a total of 273 revolutions in 1 minute to observe any potential problems associated with the samples such as micropores prior to long-term test. After the ball-on-disk tests, the volume losses were calculated with the help of 3D scanning device (Bruker ContourGT-K) and the COF graph was constructed for each sample. The ball-on-disk test results will be discussed comprehensively in Chapter 4.

## 3.5. 3D Profilometer

There are several methods in the literature to calculate the volume loss of samples after ball-on-disk test. The most common one is to measure the mass loss before and after the test. After that, volume loss can be calculated by the mass and density measurement. Another method is, more precise one, volume loss calculation by using a 3D profilometer. The working principle of a 3D profilometer is based on deformation scar caused by the wear process. Lights are reflected from different surfaces, including the reference surface and scars, and give information about the surface topography. In this study, Bruker CounterGT-K 3D (see Figure 3.6.) [45] was utilized to calculate volume losses of the samples by using its high resolution and color camera options.

Figure 3.6. 3D profilometer Bruker Contour GT-K 3D (Source: Bruker,2019)

## 3.6. Microstructural Characterization

Optical microscopy (OM), scanning electron microscopy (SEM), and transmission electron microscopy (TEM) were utilized for the characterization of the produced AMNCs. The details of these devices are given in following sections.

### 3.6.1. Optical Microscopy

Light microscopes are referred to as optical microscopes and in this study, Leica DM 2500 M optical microscope ( see Figure 3.7.) [46] is used to investigate the relatively coarse microstructural features.

Figure 3.7. Optical Microscope- Leica DM 2500 (Source: Leica, 2019)

### 3.6.2. Scanning Electron Microscopy

Unlike light microscopes, the scanning electron microscope dislodges the electrons in the outer shell of the materials by using the focused electron beam, and electrons that move from their previous position are collected with the help of suitable

detectors positioned at different locations and gives information about the microstructure and chemical composition of the material. In this research, FEI QUANTA 250 FEG device was utilized to characterize the AMNCs. (see Figure 3.8.) During the investigation of the AMNCs, different detector types were utilized. These are:

- Secondary electron (SE)
- Backscattered electron ( BSED)
- Energy dispersive x-ray (EDX)

ETD provides high resolution imaging of fine surface morphology. Because of that reason, ETD detector was utilized during the investigation of worn surface of samples to determine wear modes. BSED provides image contrast due to different atomic number of elements that are present in a material. The phases including elements with higher atomic number lead to the formation of more backscattered electron, and hence they appear brighter among the other phases.EDX is an analytical technique can be used to indentify the chemical composition of a sample.

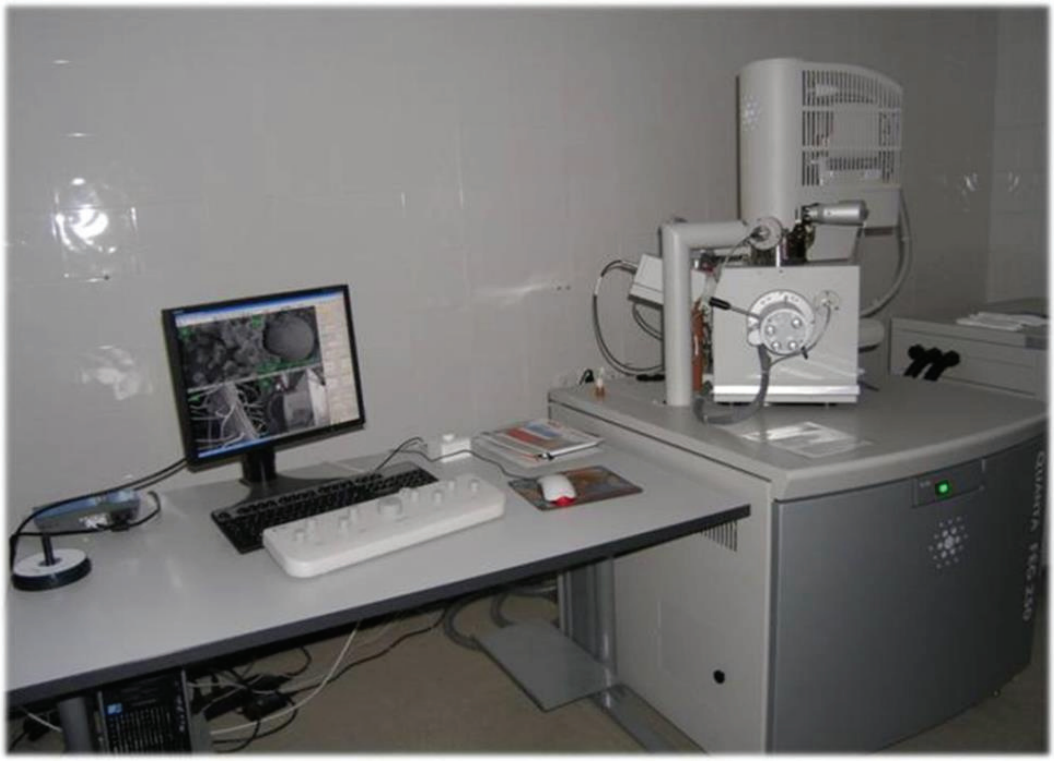

Figure 3.8. SEM device (FEI QUANTA 250 FEG)

### 3.6.3. Transmission Electron Microscopy

TEM enables to provide a higher magnification image than a light microscope and SEM and allows to examine samples with dimensions less than 100 nm. In order to produce an image in TEM, electrons must pass through the samples. Therefore, the TEM specimens have to be prepared to have a thickness of less than 100 nm. Additionally, by applying condenser lens, cyrstal structure of sample could be obtained by the paralleled electron beams [47].

Schematic arrangement of microscopic techniques (OM,SEM and TEM) is illustrated in Figure 3.9.

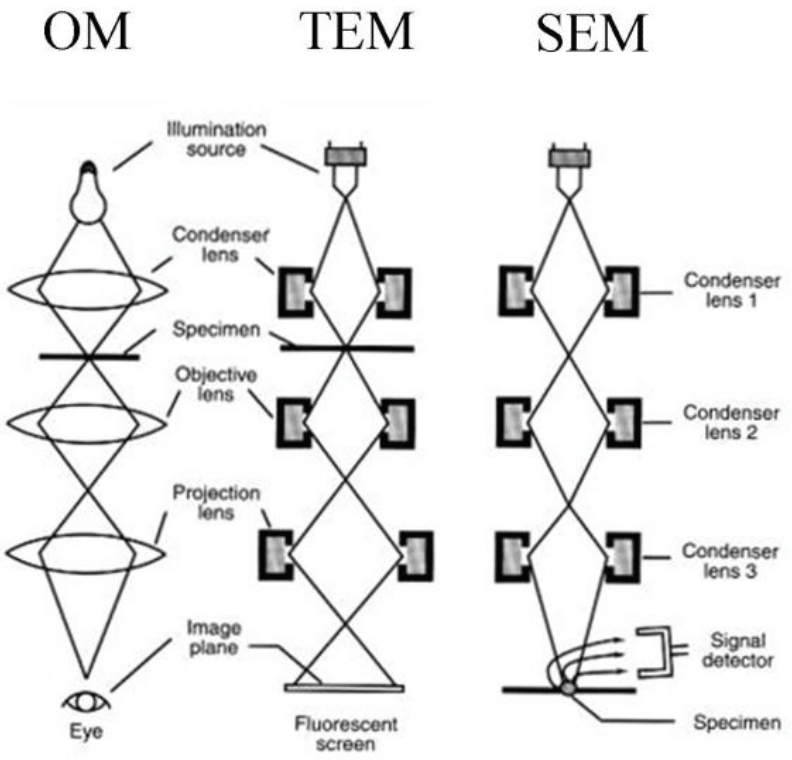


Figure 3.9.Schematic display of optical, scanning and transmission microscope methods

# Chapter 4

# RESULTS AND DISCUSSION

## 4.1. Microstructural Examination Results

In this section, microstructural examination results will be presented and discussed.

### 4.1.1. OM Results

As shown in the Figure 4.1, the microstructures of unreinforced, A360/0.25 wt.% GNPs and A360/0.5 wt.% GNPs were examined by means of an OM.

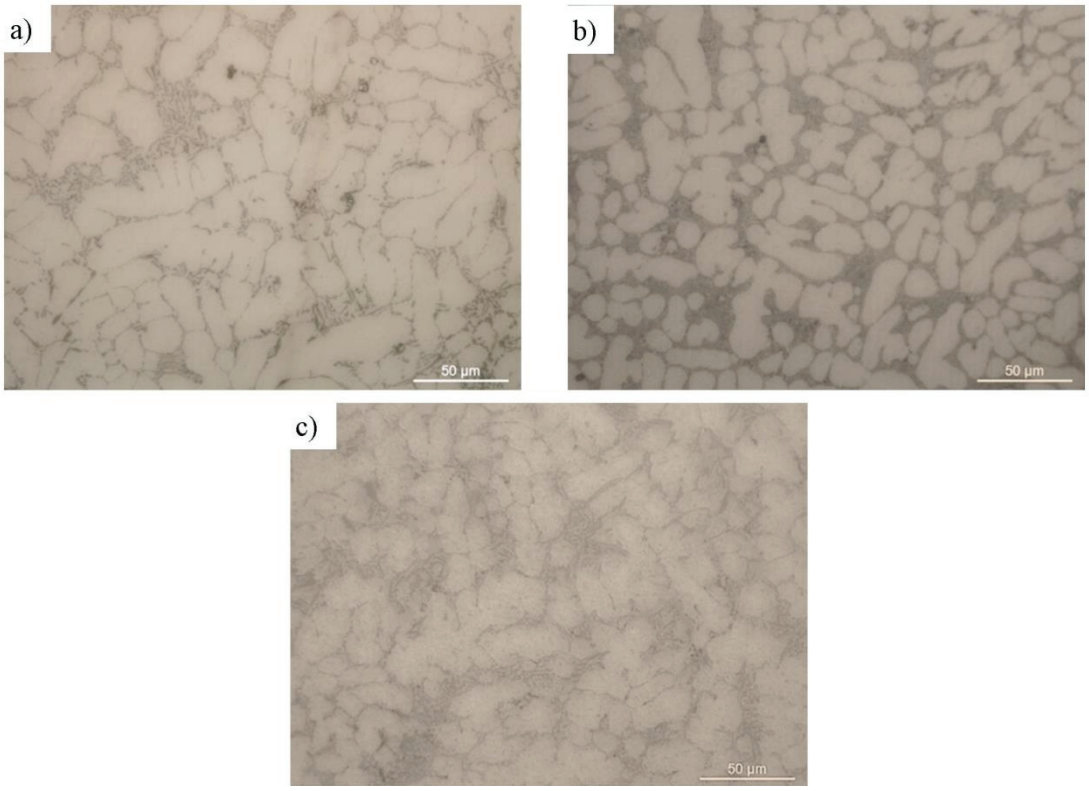


Figure 4.1. Microstructure of a) unreinforced b) A360/0.25 wt.% GNPs c) A360/0.5 wt.%GNPs

ASTM E112 was utilized to determine grain refinement effect of GNPs and the results can be seen in Figure 4.2. There are several mechanisms has been proposed that the grain size has improved by adding a secondary particles to microstructure. However, the mechanism that reduces the grain size by the addition of GNPs is that GNPs act as nucleating agents during solidification of α-Al. When the content of GNPs increases, the grain size refinement effect is weakened presumably due to the non-uniform distribution and the grain boundaries reaching the saturation point.

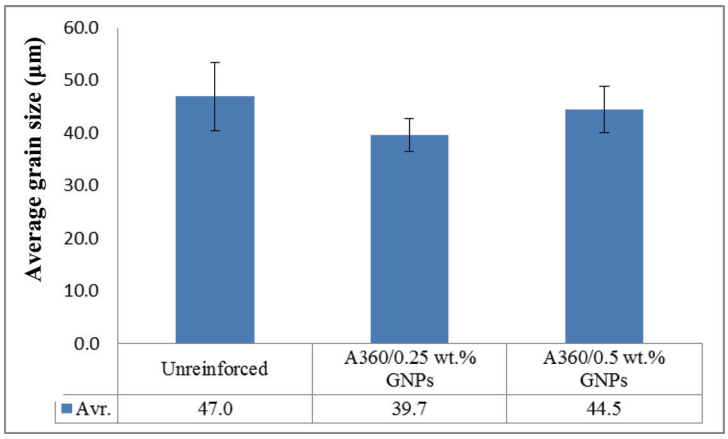


Figure 4.2. Average grain diameter of a) unreinforced b) A360/0.25 wt.% GNPs c) A360/0.5 wt.%GNPs

## 4.1.2. SEM Results

SEM was employed to document the distribution of GNPs into A360 matrix. As shown in Figure 4.3, the SEM micrographs of A360/0.25 wt.% GNPs were given at different magnifications.

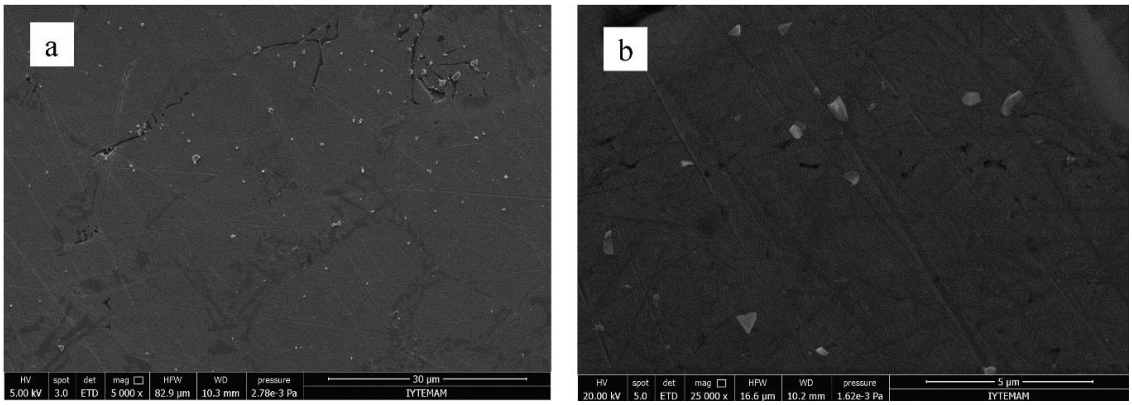


Figure 4.3. SEM micrographs of A360/0.25 wt.% GNPs in different magnifications a)5000 x b) 25000 x

The SEM micrographs show the relatively homogeneous dispersion of potential GNPs into the A360 alloy. It can be suggested that the ball milling, the mechanical stirring, and ultrasonic treatment that applied during the composite fabrication process accomplished an effective role in the distribution of GNPs. The EDX analysis in the SEM was utilized to determine whether the potential homogeneously distributed particles were GNPs. Figure 4.4. shows the EDX analysis of A360/0.25 wt.% GNPs. As seen in the second spectrum result, a high content of carbon suggests that those particles are more likely to be GNPs embedded in the matrix. It is also seen that the size of the GNPs is smaller than 5 μm, which may suggest that the average size of the GNPs is reduced during the ball milling process.

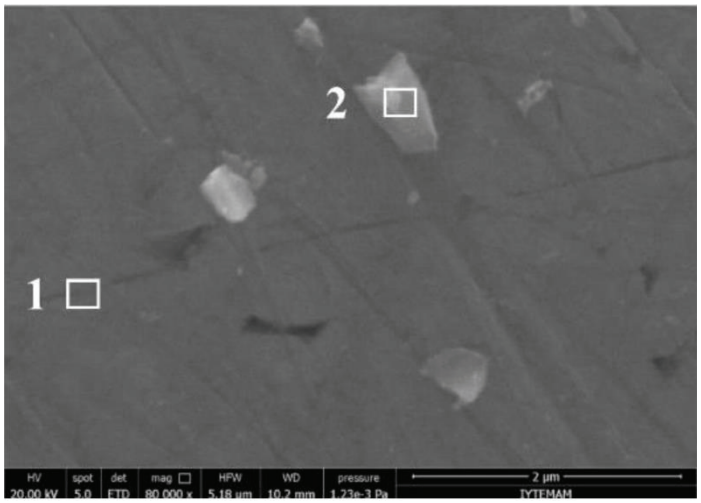


**1. Spectrum**

| Element | Wt% | Atomic % |
|---|---|---|
| Al | 86.33 | 79.83 |
| O | 11.96 | 18.65 |
| Si | 1.71 | 1.52 |
| Total: | 100.00 | 100.00 |

**2. Spectrum**

| Element | Wt% | Atomic % |
|---|---|---|
| C | 68.36 | 83.00 |
| Mg | 0.47 | 0.28 |
| Al | 26.59 | 14.37 |
| Si | 4.36 | 2.26 |
| Ca | 0.21 | 0.08 |
| Total: | 100.00 | 100.00 |

Figure 4.4. EDX results of A360/0.25 wt.% GNPs

However, when the GNPs content is increased, distribution of GNPs become a challenging task. Figure 4.5 shows the EDX map analysis of the A360/0.5 wt.% GNPs. As seen in Figure 4-5, GNPs couldn't be dispersed evenly into the matrix material. Thus, during the transferring of load, clusters of GNPs have a negative effect on the mechanical properties. Particularly, wear behavior is examined, clustered GNPs could lead a high volume loss due to the effortless detachment of GNPs clusters from the surface.

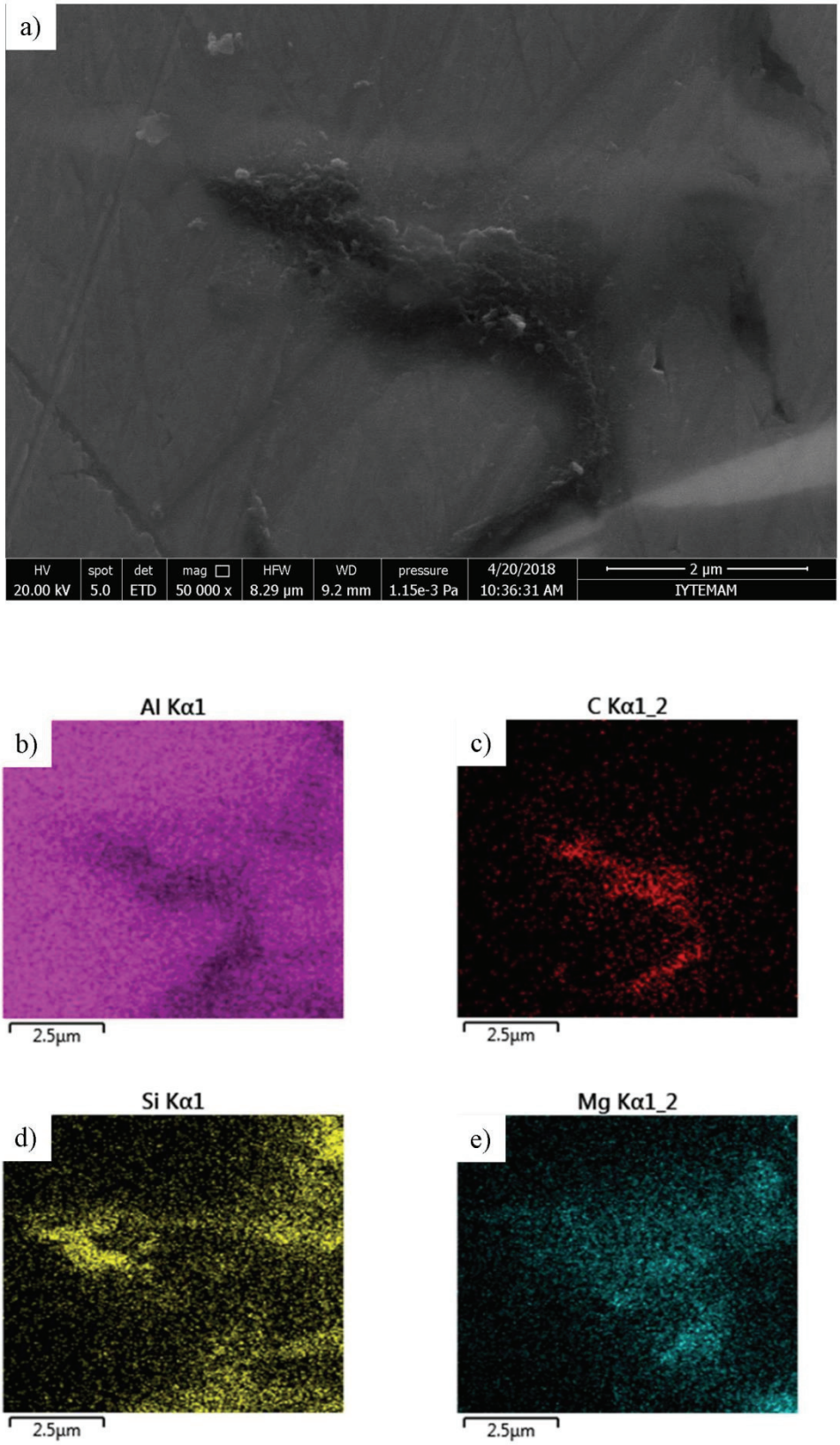


Figure 4.5. EDX mapping of A360 / 0.5 wt.% GNPs

### 4.1.3. TEM Results

In order to clarify whether GNPs interacted with A360 alloy during the fabrication process, TEM was used. The TEM observation of the A360/0.25 wt.% GNPs nanocomposite is given in Figure 4.6. According to the TEM images, Figure 4.6a proves that GNPs have been succesfully embedded into the aluminum matrix vertically. In addition, the interlayer between the GNPs is characteristic, and the high resolution of TEM enables us to measure the distance between this interlayer. As shown in Figure 4.6b, an interlayer of graphene was found to be 0.34 nm. It was previously reported that the distance of graphene layers is equal to 0.34 nm[25] which is consistent with our findings. Also, Figure 4-6-b demonstrates that no void or second phase has existed between the aluminum matrix and GNPs, indicating that a clean bonding was achieved to effectively transfer the load from the matrix to the GNP.

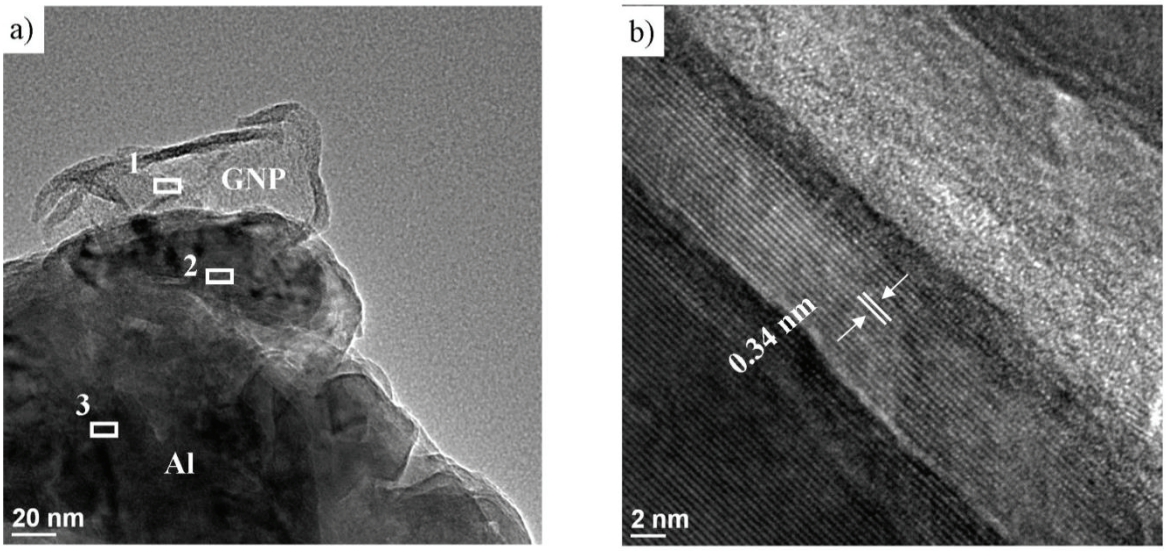


Figure 4.6. TEM images of A360/0.25 wt.% GNPs nanocomposite b) Distance of graphene interlayer

Additionally, EDX analyses were applied to determine presence of GNPs and the results were given in Figure 4.7. As seen in Figure 4.7a (Spectrum 1), relatively high content of C suggests that the particle which is embedded into the matrix vertically, is GNP. Figure 4.7b (Spectrum 2) was also taken from the matrix-GNP interface. Al, O and C peaks were observed. This result showed that the bonding was clean and there is no secondary phase formed. In the last analysis (Figure 4.7c), the Si peak was observed

as well as Al. The reason for this is that the A360 alloy contains 10% by weight of Si as shown in the Table 3.1.

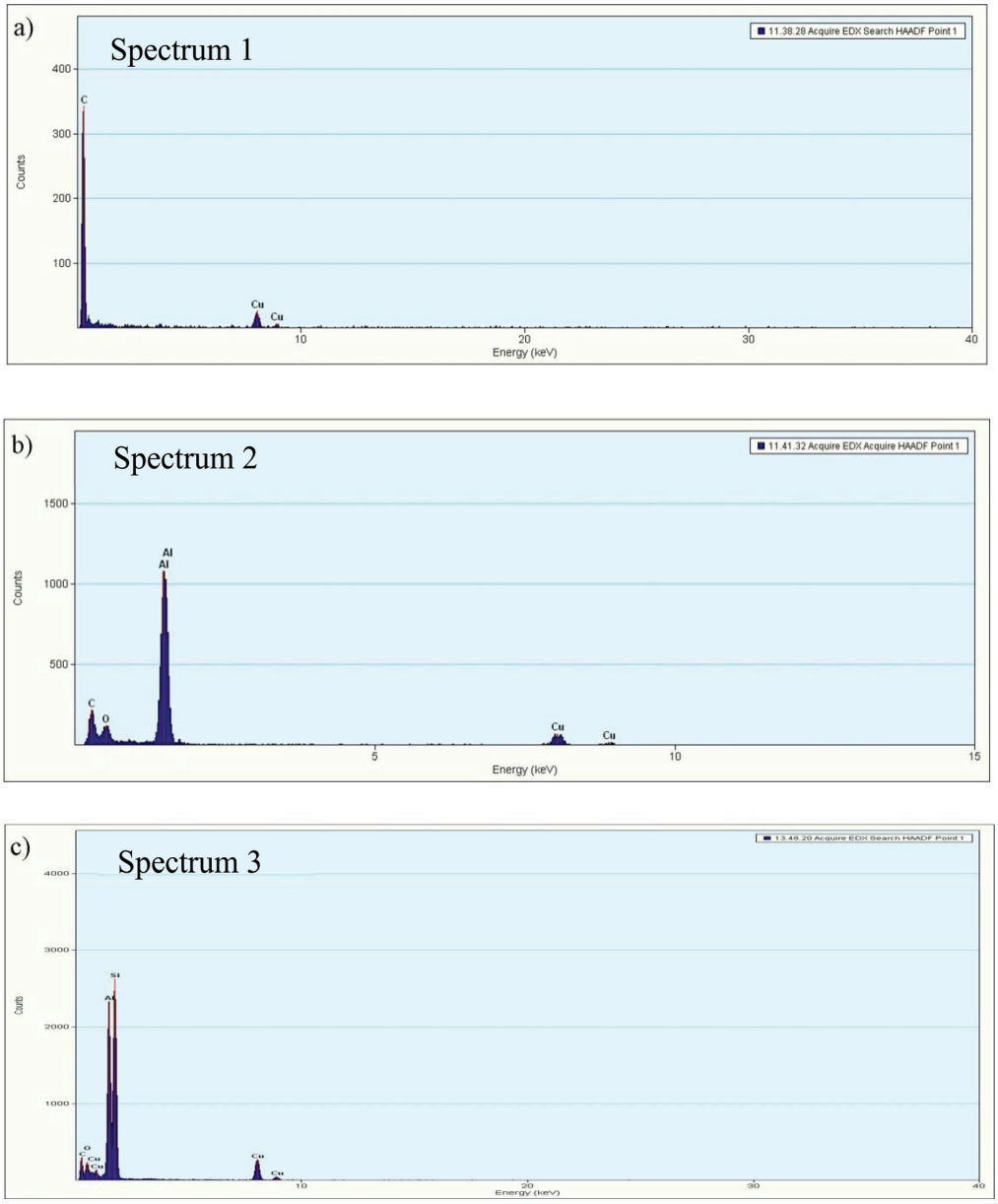


Figure 4.7. EDX results of A360/0.25 wt.% GNPs from three diferent location

## 4.2. Hardness Results

In order to determine Vickers hardness of the samples, tests were carried out by means of Shimadzu Micro Hardness Tester (HMV) at room tempterature. Five tests were performed for each sample and Figure 4.8 was obtained by taking the averages.

Considering the results, GNPs reinforced nanocomposites showed better hardness performance than unreinforced alloy. The enhancement in hardness can be attributed to reasonably dispersing of the GNPs into the Al matrix, and hence grain refinement was accomplished by means of GNPs.

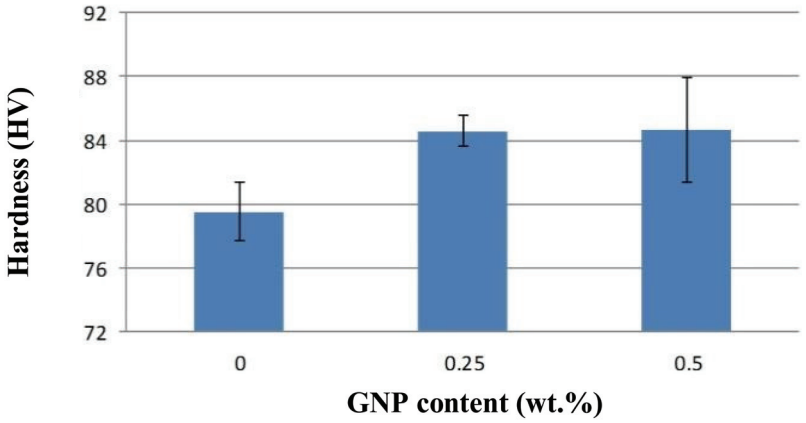


Figure 4.8. Hardness results of the unreinforced alloy and the composites with A360/0.25 wt.% GNPs and A360/0.25 wt.% GNPs at room temperature

## 4.4. Ball-on-disk Test Results

During the ball-on-disk tests, COF values were transformed into to a graph as a function of time. A representative COF graph for a sample worn at RT was given in Figure 4.9.

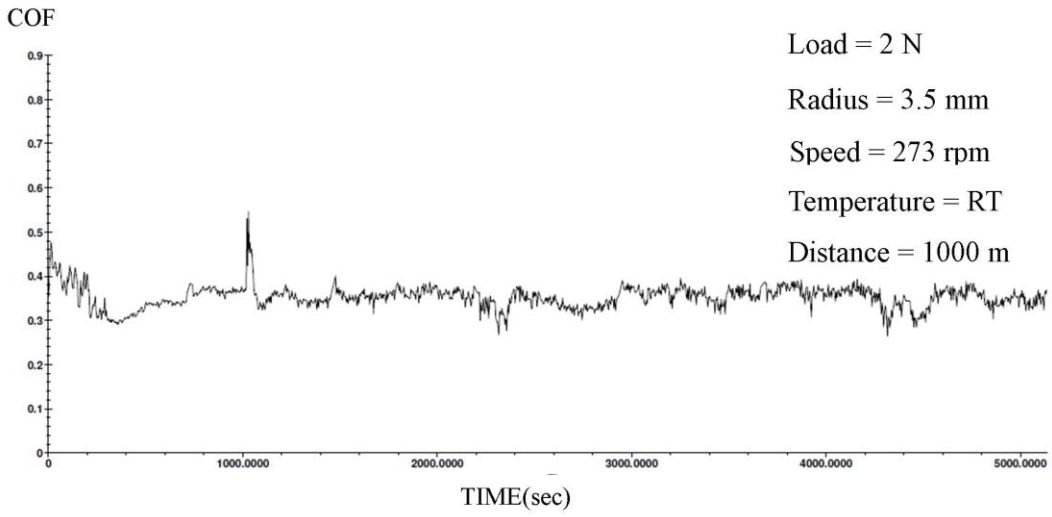


Figure 4.9. COF results of unreinforced sample at RT.

Test parameters were kept constant and three tests were performed for each sample at three different temperatures, and average COF values were obtained. These results are reported in Figure 4.10.

Depending on the GNP content and temperature, unreinforced alloy and

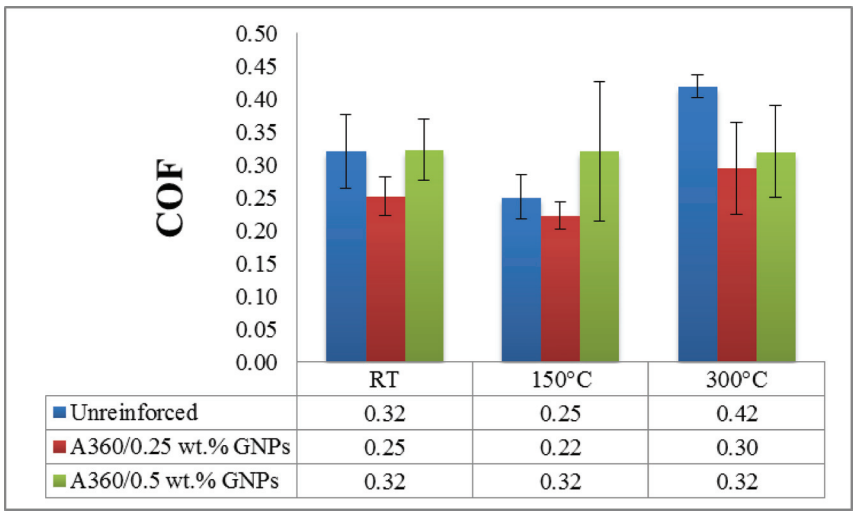


| | RT | 150°C | 300°C |
|---|---|---|---|
| Unreinforced | 0.32 | 0.25 | 0.42 |
| A360/0.25 wt.% GNPs | 0.25 | 0.22 | 0.30 |
| A360/0.5 wt.% GNPs | 0.32 | 0.32 | 0.32 |

Figure 4.10. Average COF results of unreinforced and nanocomposite samples

nanocomposites exhibited varying results. As shown in Figure 4.10, a decrease in COF was observed with increasing temperature from RT to 150°C for two samples except A360/0.5 wt.% GNPs sample. Because of the increase in temperature, the oxidation rate on the surface of the samples increased and this layer was considered to act as a protective layer during the wear, and hence it may be the reason for reduced volume losses and relatively low COF values. A360/0.25 wt.% GNPs nanocomposites have the lower COF values than those of A360/0.5 wt.% GNPs nanocomposites and unreinforced alloy in all conditions which verifies the results of volume loss and the role of GNPs effectively embedded in A360/0.25 wt.% GNPs nanocomposite as a lubricant. As seen in Figure 4.13, it can be interpreted that the decrease in the COF values affected the volume losses in a positive direction. So, the presence of GNPs on the contact surface of A360/0.25 wt.% GNPs samples may be much more available than A360/0.5 wt.% GNPs. During the sliding process, the potential GNPs of A360/0.5 wt.% GNPs could not be released and covered contact surface as a solid lubricant due to the lack of homogeneity. Therefore, A360/0.25 wt.% GNPs samples may exhibit reduced COF than A360/0.5 wt.% GNPs, and hence this results is corelated with SEM investigation, as shown in Figure 4.5. At 300°C, the increase in temperature results in aluminum softening which increases the contact area even at low loads, and hence COF increased.

## 4.3. 3D Profilometer Results

Bruker Contour GT-K 3D optical microscope was used to calculate the volume loss of each sample. A seen in Figure 4.11, it enables to see 3D, 2D modeling of sample and wear profile separately.

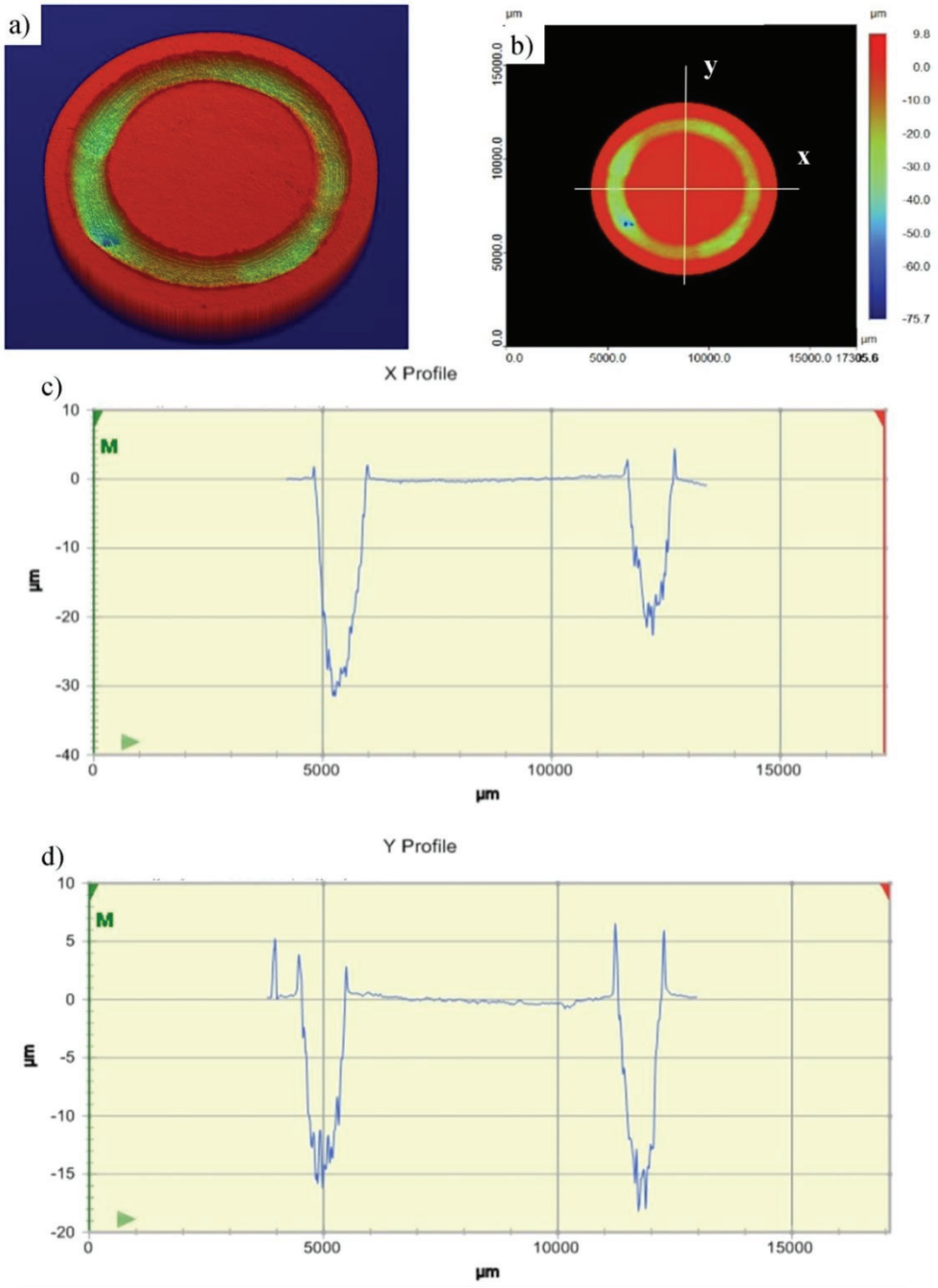


Figure 4.11 a) 3D model of unreinforced alloy, b) 2D model of scanned surface, c-d) X and Y profiles

The total volume loss of the samples is obtained by calculating the overall deflection in X and Y axis by means of software. For each sample, volume loss analysis was performed at different temperatures as shown in the Figure 4.12. According to the results, and average volume loss data versus temperature and GNP content in the composites was constructed, as shown in Figure 4.13.

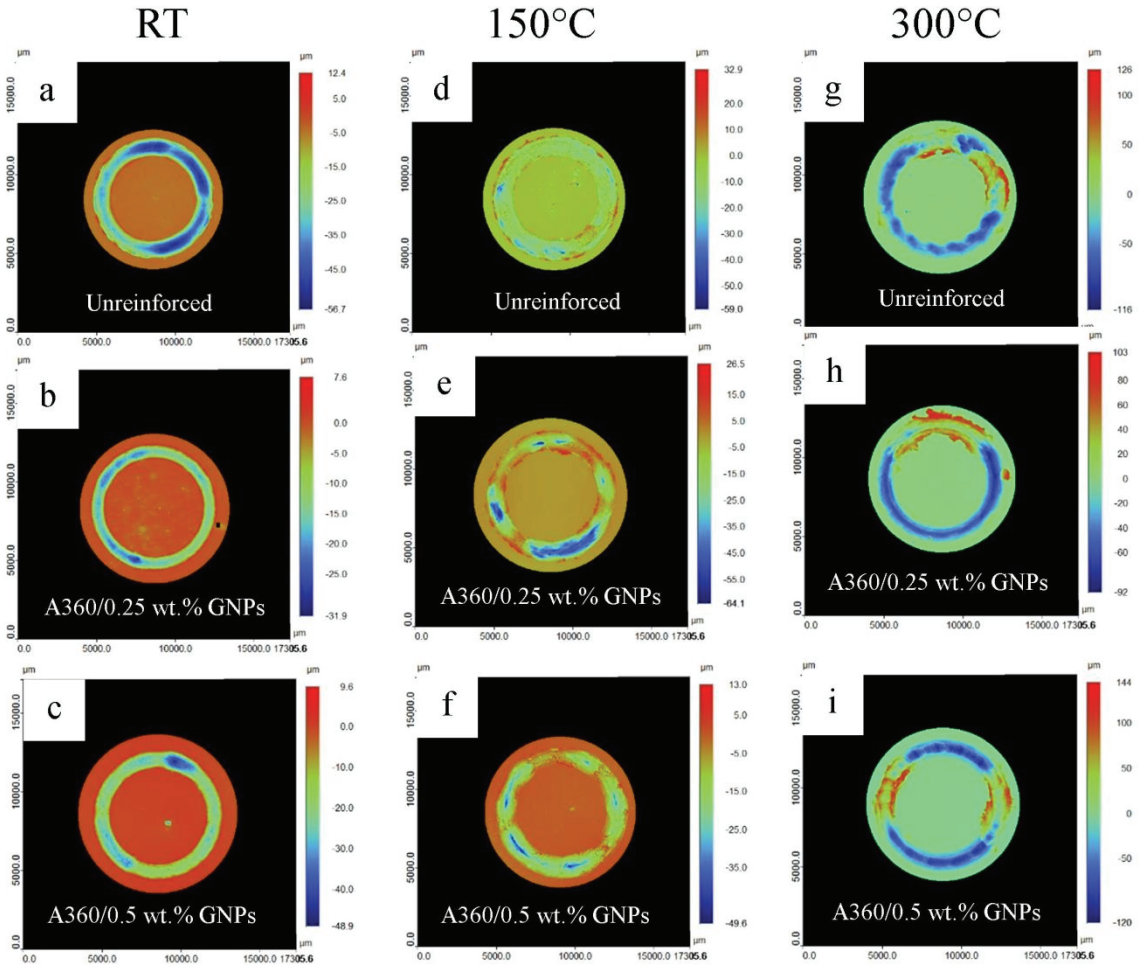


Figure 4.12. 3D scanned surface of unreinforced and nanocomposite samples tested at different temperatures

When the results are evaluated at RT, A360/0.25 wt.% GNPs nanocomposites have the narrowest and shallowest wear scar. This observation is consistent with the volume loss data provided in Figure 4.13 as A360/0.25 wt.% GNPs performed the lowest volume loss at RT. However, A360/0.5 wt.% GNPs exhibited the greatest volume loss result among the other samples. It can be attributed to the fact that clusters and unevenly dispersion of GNPs observed in the microstructure led to relatively weak

microstructure and hence A360/0.5 wt.% GNPs samples were prone to wear and worn easily.

At 150 ° C, due to the increased oxidation rate, a protective and relatively harder interface is more likely to formed between counterface and samples. Therefore, it can be deduced that volume loss reduced when the results are compared with the other samples worn at RT. When unreinforced, A360/0.25 wt.% GNPs and A360/0.5 wt.% GNPs were compared, A360/0.5 wt.% GNPs showed the highest volume loss as expected due to its relatively high content of GNP clusters.

Where the temperature exceeds to 250° C, the microstructure of aluminum alloys is not stable [44]. Therefore, during wear, a dramatic increase in volume loss is observed compared to the test conducted at RT and 150 ° C. This may have resulted in the emergence of GNPs on the sample surface after the wear of aluminum matrix, a potential solid lubricant embedded in the matrix, and caused the loss of volume of the nanocomposites to be less than the reference sample without GNPs.

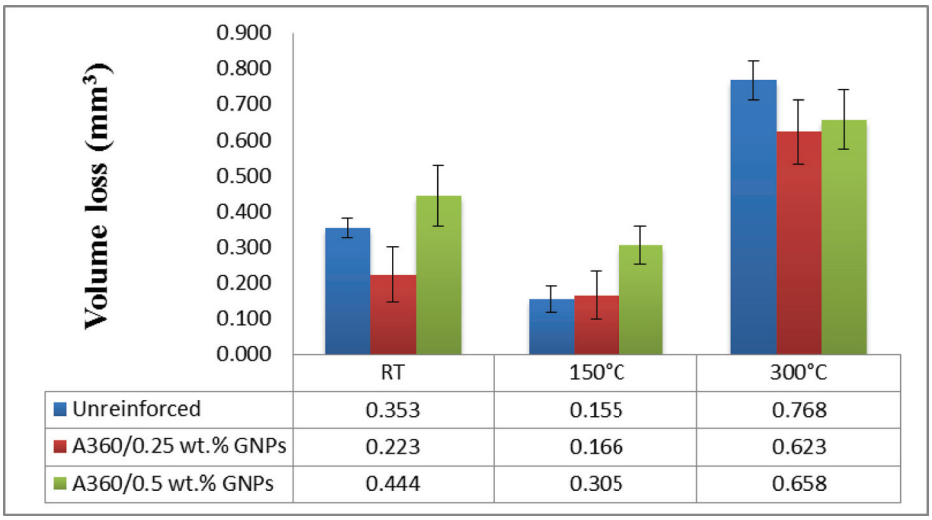


| | RT | 150°C | 300°C |
|---|---|---|---|
| Unreinforced | 0.353 | 0.155 | 0.768 |
| A360/0.25 wt.% GNPs | 0.223 | 0.166 | 0.623 |
| A360/0.5 wt.% GNPs | 0.444 | 0.305 | 0.658 |

Figure 4.13. Average volume losses of unreinforced and nanocomposite samples worn at different temperatures

## 4.5. Analyses of Worn Surfaces

The sample surfaces were examined by SEM to determine the wear modes and they suggest the presence of GNP on worn surfaces. Figure 4.14 shows the SEM micrographs of samples at RT. When the worn surfaces of all samples were investigated at RT, it is revealed that all scratch marks were found to be parallel to the sliding direction. Fine grooves and ploughing marks indicate that abrasive wear mechanism is

the predominant wear mechanism during the tests [48,49]. Additionally, due to the existence of delamination patches on the worn surfaces for all samples, it can be implied that the other wear mechanism could be adhesive wear mechanism. Moreover, due to the solid lubricant effect of the GNPs, the worn surface of A360/0.25 wt.% GNP nanocomposites has a more smoother worn surface compare to the others, and this is corelated with the reduced COF and volume loss results, as seen in Figure 4-10 and 4-13.

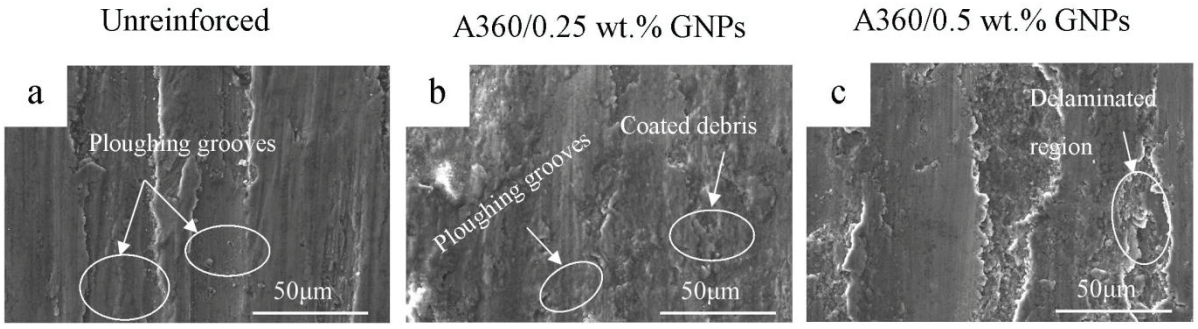


Figure 4.14. Worn surfaces of unreinforced and nanocomposite samples at RT

At 150°C, it is thought that the oxidation rate increased and the oxide film caused a reduction in volume loss by preventing metal-metal contact during the wear [50]. At the same time, the oxide particles may have pulled out the GNPs in the composites while abrading the soft material, which may have induced a reduction in the COF by forming a temporary solid-lubricant film on the worn surfaces. Among the samples, the smooethest and less deformed surface belongs to A360/0.25 wt.% GNP nanocomposites, as shown in Figure 4-15. Further, the particles that are likely to be oxides may suggest that the wear mechanism is oxidation wear, as shown in Figures 4.15.

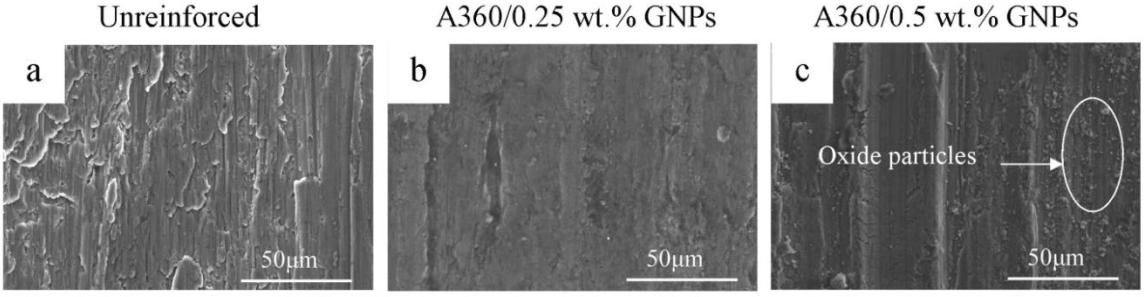


Figure 4.15. Worn surfaces of unreinforced and nanocomposites at 150°C

At 300°C, aluminum and its alloys started softening, the protective oxide layer at the worn surface cannot remain stable as the amount of plastic deformation is large. This can usher in the wear mechanism to transform from mild to severe wear. Additonally, it can be observed that considerable severe wear occurred due to the laminated-shaped wear debris found on the surface of the samples, as seen in Figure 4.16a. This situation is more likely to both the COF and volume loss. (see Figure 4.10 and Figure 4.13)

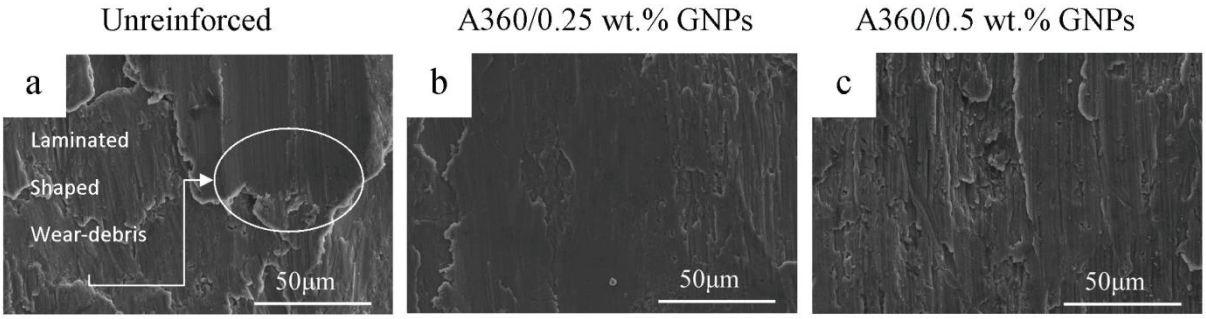


Figure 4.16. Worn surfaces of the unreinforced and nanocomposites at 300°C.

In addition, the EDX analysis was also performed on the surface of the A360/0.25 wt.% GNP nanocomposites to locate the potential GNPs in the vicinity of the worn surface, in Figure 4.17. As a result of a point EDX analysis, a substantial carbon peak suggests that the spectrum in which EDX analysis was performed is more likely to contain the GNPs.

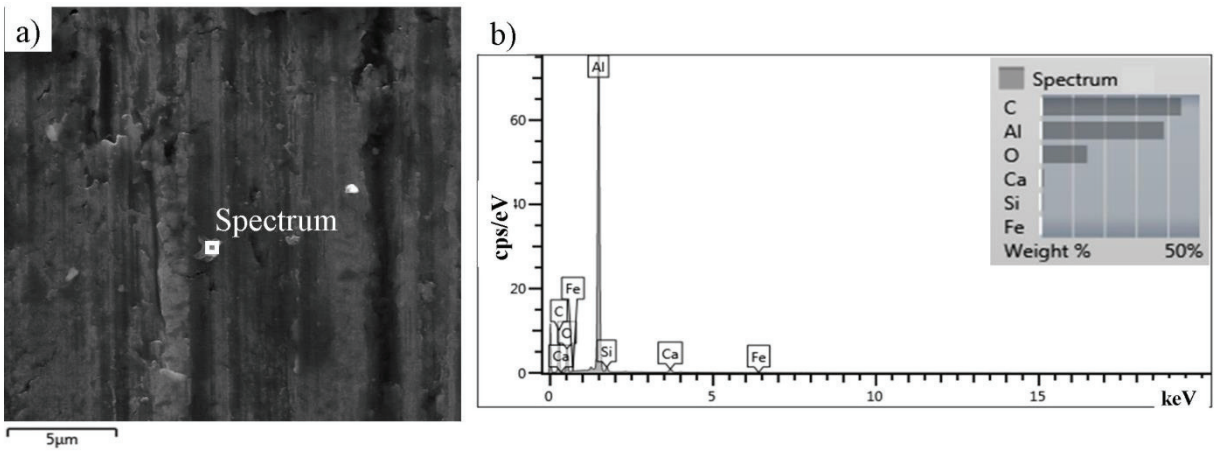


Figure 4.17. EDX analysis of worn surface of A360/0.25 wt.% GNP nanocomposite.

# Chapter 5

# CONCLUSIONS

The experimental results indicate that the stir casting method with the application of ultrasounds has been found to be promising method for the distribution of GNPs into the A360 matrix. The SEM results of fabricated nanocomposites with 0.25 and 0.5 wt.% GNPs show that a relatively uniform dispersion and distribution of reinforcement into the matrix was achieved for 0.25 wt.% content. When the content of GNPs exceeded 0.25 wt.%, GNPs clusters were observed, and hence it led to the diminishing of mechanical and tribological properties.

The average grain sizes of unreinforced, A360/0.25 wt.% GNP nanocomposites and A360/0.5 wt.% GNP nanocomposites were measured and results were found to be 47 μm, 39.7 μm, and 44.5 μm respectively. The results indicates that the grain size of A360 matrix was reduced by 16% with the incorporation of 0.25 wt.% GNPs. The main reason for this improvement could be the GNP acts as a nuclei during solidification.

The Vickers hardness test results of unreinforced, A360/0.25 wt.% GNP and A360/0.5 wt.% GNP nanocomposites were calculated to be 76 HV, 86 HV ve 85 HV respectively. The improvement in the hardness results can be ascribed to a relatively homogeneous dispersion of GNPs, and hence the grain refinement of the A360 alloy by GNPs.

TEM images of A360/0.25 wt.% GNPs show that there is no void or secondary phase formed between the A360 matrix and the GNPs, which may suggest that no chemical reaction took place at the interface and that a clean bonding was obtained to effectively transfer the load from the matrix to the GNP.

By adding 0.25 wt. %GNPs into the A360 matrix, the COF was decreased by 21.88 % at RT. The enhancement in the COF may be attributed to the solid lubricant effect of GNPs which were found to be uniformly dispersed through the matrix. In addition, the volume loss of A360 matrix decreased by 36.83% with the 0.25 GNP addition due to the development in COF at RT and hard nature of GNPs. At 150°C, besides the presence of GNPs, the oxidation was considered to be a also critical phenomena to evaluate the COF and volume loss results. The addition of 0.25 wt.% GNPs, 12% decrease was determined in the COF. However, 7.1% volume loss

increment was observed suprisingly. At 300°C, the COF and volume loss were found to reduce by 28.57% and 18.8% with 0.25 wt.% GNP respectively. The reason for the observation of a higher loss of volume in all sample at 300°C is the softening of the matrix material.

Due to the presence of fine grooves, ploughing marks, and delamination patches, abrasive and adhesive mechanism were suggested to be main wear mechanisms at RT. The worn surface of A360/0.25 wt.% GNP nanocomposites was found to be smoother than those of other samples. At 150°C, the SEM examination of worn surfaces showed that oxidation wear mechanism was the dominant wear mechanism in the unreinforced alloy and nanocomposites. At 300°C, the laminated wear debris observed on the worn surfaces could be the evidence for that the wear mechanism transformed from mild to severe.

# REFERENCES


(1) Holmberg, K.; Andersson, P.; Erdemir, A. Global Energy Consumption Due to Friction in Passenger Cars. *Tribol. Int.* **2012**, *47*, 221–234. https://doi.org/10.1016/j.triboint.2011.11.022.

(2) Tjong, S. C. Recent Progress in the Development and Properties of Novel Metal Matrix Nanocomposites Reinforced with Carbon Nanotubes and Graphene Nanosheets. *Mater. Sci. Eng. R Reports* **2013**, *74* (10), 281–350. https://doi.org/10.1016/j.mser.2013.08.001.

(3) Donnet, C.; Erdemir, a. Solid Lubricant Coatings: Recent Developments and Future Trends. *Tribol. Lett.* **2004**, *17* (3), 389–397. https://doi.org/10.1023/B:TRIL.0000044487.32514.1d.

(4) Donnet, C.; Erdemir, A. Historical Developments and New Trends in Tribological and Solid Lubricant Coatings. *Surf. Coatings Technol.* **2004**, *180–181*, 76–84. https://doi.org/10.1016/j.surfcoat.2003.10.022.

(5) Akbari, M. K.; Baharvandi, H.; Mirzaee, O. Investigation of Particle Size and Reinforcement Content on Mechanical Properties and Fracture Behavior of A356-$Al_2O_3$ Composite Fabricated by Vortex Method. *J. Compos. Mater.* **2014**, *48* (27), 3315–3330. https://doi.org/10.1177/0021998313507618.

(6) Ibrahim, I. A.; Mohamed, F. A.; Lavernia, E. J. Particulate Reinforced Metal Matrix Composites - a Review. *J. Mater. Sci.* **1991**, *26* (5), 1137–1156. https://doi.org/10.1007/BF00544448.

(7) Alipour, M.; Eslami-Farsani, R. Synthesis and Characterization of Graphene Nanoplatelets Reinforced AA7068 Matrix Nanocomposites Produced by Liquid Metallurgy Route. *Mater. Sci. Eng. A* **2017**, *706* (June), 71–82. https://doi.org/10.1016/j.msea.2017.08.092.

(8) Dorri Moghadam, A.; Omrani, E.; Menezes, P. L.; Rohatgi, P. K. Mechanical and Tribological Properties of Self-Lubricating Metal Matrix Nanocomposites Reinforced by Carbon Nanotubes (CNTs) and Graphene - A Review. *Compos. Part B Eng.* **2015**, *77*, 402–420. https://doi.org/10.1016/j.compositesb.2015.03.014.

(9) Yang, Y.; Lan, J.; Li, X. Study on Bulk Aluminum Matrix Nano-Composite Fabricated by Ultrasonic Dispersion of Nano-Sized SiC Particles in Molten Aluminum Alloy. *Mater. Sci. Eng. A* **2004**, *380* (1), 378–383. https://doi.org/10.1016/j.msea.2004.03.073.

(10) Hassan, S. F.; Gupta, M. Effect of Nano-ZrO2particulates Reinforcement on Microstructure and Mechanical Behavior of Solidification Processed Elemental Mg. *J. Compos. Mater.* **2007**, *41* (21), 2533–2543. https://doi.org/10.1177/0021998307074187.

(11) Novoselov, K. S.; Geim, A. K.; Morozov, S. V; Jiang, D. Electric Field Effect in Atomically Thin Carbon Films. **2004**, *306* (October), 666–669.

(12) Lee, C.; Wei, X.; Kysar, J. W.; Hone, J. Measurement of the Elastic Properties and Intrinsic Strength of Monolayer Graphene. *Science (80-. ).* **2008**, *321* (5887), 385–388. https://doi.org/10.1126/science.1157996.

(13) Chawla, K. K.; Chawla, N. *Metal-Matrix Composites*; 2004. https://doi.org/10.1016/B978-0-08-050073-7.50011-7.

(14) Evans, A.; Marchi, C. S.; Mortensen, A. *Metal Matrix Composites in Industry: An Introduction and a Survey*, 1st ed.; Kluwer Academic: Newyork, 2003. https://doi.org/10.1887/0750308729/b1149c3.

(15) Kainer, K. U. *Metal Matrix Composites: Custom-Made Materials for Automotive and Aerospace Engineering*; 2006.

(16) CLYNE, T. W. An Introductory Overview of MMC Systems, Types, and Developments. *Compr. Compos. Mater.* **2004**. https://doi.org/10.1016/b0-08-

042993-9/00001-2.

(17) Prasad, S. V.; Asthana, R. Aluminum Metal-Matrix Composites for Automotive Applications: Tribological Considerations. *Tribol. Lett.* **2004**, *17* (3), 445–453. https://doi.org/10.1023/B:TRIL.0000044492.91991.f3.

(18) Kumar, G. B. V.; Rao, C. S. P.; Selvaraj, N. Mechanical and Tribological Behavior of Particulate Reinforced Aluminum Metal Matrix Composites – a Review. *J. Miner. Mater. Charact. Eng.* **2015**, *10* (01), 59–91. https://doi.org/10.4236/jmmce.2011.101005.

(19) Chen, R.; Iwabuchi, A.; Shimizu, T.; Shin, H. S.; Mifune, H. The Sliding Wear Resistance Behavior of NiAl and SiC Particles Reinforced Aluminum Alloy Matrix Composites. *Wear* **1997**, *213* (1–2), 175–184. https://doi.org/10.1016/S0043-1648(97)00123-3.

(20) Berman, D.; Erdemir, A.; Sumant, A. V. Graphene: A New Emerging Lubricant. *Mater. Today* **2014**, *17* (1), 31–42. https://doi.org/10.1016/j.mattod.2013.12.003.

(21) Baradeswaran, A.; Elaya Perumal, A. Effect of Graphite on Tribological and Mechanical Properties of AA7075 Composites. *Tribol. Trans.* **2015**, *58* (1), 1–6. https://doi.org/10.1080/10402004.2014.947663.

(22) Shanmughasundaram, P.; Subramanian, R. Wear Behaviour of Eutectic Al-Si Alloy-Graphite Composites Fabricated by Combined Modified Two-Stage Stir Casting and Squeeze Casting Methods. *Adv. Mater. Sci. Eng.* **2013**, *2013*, 1–8. https://doi.org/10.1155/2013/216536.

(23) Mazahery, A.; Abdizadeh, H.; Baharvandi, H. R. Development of High-Performance A356/Nano-Al2O3composites. *Mater. Sci. Eng. A* **2009**, *518* (1–2), 61–64. https://doi.org/10.1016/j.msea.2009.04.014.

(24) Randviir, E. P.; Brownson, D. A. C.; Banks, C. E. A Decade of Graphene Research: Production, Applications and Outlook. *Mater. Today* **2014**, *17* (9), 426–432. https://doi.org/10.1016/j.mattod.2014.06.001.

(25) Dong, H. S.; Qi, S. J. Realising the Potential of Graphene-Based Materials for Biosurfaces – A Future Perspective. *Biosurface and Biotribology* **2015**, *1* (4), 229–248. https://doi.org/10.1016/j.bsbt.2015.10.004.

(26) Ghazaly, A.; Seif, B.; Salem, H. G. Mechanical and Tribological Properties of AA2124-Graphene Self Lubricating Nanocomposite. *Miner. Met. Mater. Ser.* **2016**, No. 210869, 411–415. https://doi.org/10.1007/978-3-319-65136-1_71.

(27) Tabandeh-Khorshid, M.; Omrani, E.; Menezes, P. L.; Rohatgi, P. K. Tribological Performance of Self-Lubricating Aluminum Matrix Nanocomposites: Role of Graphene Nanoplatelets. *Eng. Sci. Technol. an Int. J.* **2016**, *19* (1), 463–469. https://doi.org/10.1016/j.jestch.2015.09.005.

(28) Young, T. An Essay on the Cohesion of Fluids. Philosophical Transactions of Royal Society. *The Sublime* **1805**, 65–87. https://doi.org/10.1017/cbo9780511620409.035.

(29) Nuriel, S.; Liu, L.; Barber, A. H.; Wagner, H. D. Direct Measurement of Multiwall Nanotube Surface Tension. *Chem. Phys. Lett.* **2005**, *404* (4–6), 263–266. https://doi.org/10.1016/j.cplett.2005.01.072.

(30) Oh, S. Il; Lim, J. Y.; Kim, Y. C.; Yoon, J.; Kim, G. H.; Lee, J.; Sung, Y. M.; Han, J. H. Fabrication of Carbon Nanofiber Reinforced Aluminum Alloy Nanocomposites by a Liquid Process. *J. Alloys Compd.* **2012**, *542*, 111–117. https://doi.org/10.1016/j.jallcom.2012.07.029.

(31) Omrani, E.; Moghadam, A. D.; Menezes, P. L.; Rohatgi, P. K. Influences of Graphite Reinforcement on the Tribological Properties of Self-Lubricating Aluminum Matrix Composites for Green Tribology, Sustainability, and Energy Efficiency—A Review. *Int. J. Adv. Manuf. Technol.* **2016**, *83* (1–4), 325–346. https://doi.org/10.1007/s00170-015-7528-x.

(32) Silvain, J. F.; Proult, A.; Lahaye, M.; Douin, J. Microstructure and Chemical Analysis of C/Cu/Al Interfacial Zones. *Compos. Part A Appl. Sci. Manuf.* **2003**, *34* (12), 1143–1149. https://doi.org/10.1016/j.compositesa.2003.08.006.

(33) D.Hull; Bacon, D.J. *Introduction to Dislocations*, 5th ed. Butterworth-Heinemann ISBN: 978-0-08-096672-4

(34) Lloyd, D. J. Particle Reinforced Aluminium and Magnesium Matrix Composites. *Int. Mater. Rev.* **2014**, *39* (1), 1–23. https://doi.org/10.1179/imr.1994.39.1.1.

(35) Zhang, Z.; Chen, D. L. Consideration of Orowan Strengthening Effect in Particulate-Reinforced Metal Matrix Nanocomposites: A Model for Predicting Their Yield Strength. *Scr. Mater.* **2006**, *54* (7), 1321–1326. https://doi.org/10.1016/j.scriptamat.2005.12.017.

(36) Casati, R.; Vedani, M. Metal Matrix Composites Reinforced by Nano-Particles—A Review. *Metals (Basel).* **2014**, *4* (1), 65–83. https://doi.org/10.3390/met4010065.

(37) Suresh, S.; Mortensen, A.; Needleman, A. *Fundamentals of Metal-Matrix Composites*; Butterworth-Heinemann: Boston, 1993.

(38) Stachowiak, G. W. *Wear: Materials, Mechanisms and Practice*; John Wiley & Sons, 2004. ISBN-13: 978-0-470-01628-2

(39) Hutchings, I.; Shipway P. *Tribology Friction and Wear of Engineering Materials*, 2nd ed. http://dx.doi.org/10.1016/B978-0-08-100910-9.00003-9

(40) Kato, K.; Adachi, K. 7.1 Wear Mechanisms. **2001**, 1–28.

(41) Archard, J. F. Contact and Rubbing of Flat Surfaces. *J. Appl. Phys.* **1953**, *24* (8), 981–988. https://doi.org/10.1063/1.1721448.

(42) Kaufman, J. G.; Rooy, E. L. *Castings Properties , Processes , and Applications*; 2004.

(43) Lee, J. C.; Byun, J. Y.; Park, S. B.; Lee, H. I. Prediction of Si Contents to Suppress the Formation of Al4C3 in the SiCp/Al Composite. *Acta Mater.* **1998**, *46* (5), 1771–1780. https://doi.org/10.1016/S1359-6454(97)00265-6.

(44) Rajaram, G.; Kumaran, S.; Rao, T. S. High Temperature Tensile and Wear Behaviour of Aluminum Silicon Alloy. *Mater. Sci. Eng. A* **2010**, *528* (1), 247–253. https://doi.org/10.1016/j.msea.2010.09.020.

(45) High-performance scientific instruments and solutions for molecular and materials research, as well as for industrial and applied analysis. http://www.bruker.com/ (accessed June 8, 2019).

(46) Leica Women Foto Project: Award Apply Now https://us.leica-camera.com/ (accessed June 8, 2019).

(47) Tang, C. Y.; Yang, Z. *Transmission Electron Microscopy (TEM)*; Elsevier B.V., 2017. https://doi.org/10.1016/B978-0-444-63776-5.00008-5.

(48) Zhang, A.; Han, J.; Su, B.; Li, P.; Meng, J. Microstructure, Mechanical Properties and Tribological Performance of CoCrFeNi High Entropy Alloy Matrix Self-Lubricating Composite. *Mater. Des.* **2017**, *114*, 253–263. https://doi.org/10.1016/j.matdes.2016.11.072.

(49) Zafari, A.; Ghasemi, H. M.; Mahmudi, R. Tribological Behavior of AZ91D Magnesium Alloy at Elevated Temperatures. *Wear* **2012**, *292–293*, 33–40. https://doi.org/10.1016/j.wear.2012.06.002.

(50) Bai, Pramila Biswas, S. . Effect of Magnesium Addition and Heat Treatment on Mild Wear of Hypoeutectic Aluminium-Silicon Alloys. **1991**, *39* (5), 833–840.